PHYSICAL REVIEW B **87**, 195427 (2013)

Nonlocal transport properties of nanoscale conductor–microwave cavity systems

C. Bergenfeldt and P. Samuelsson
Division of Mathematical Physics, Lund University, Box 118, S-221 00 Lund, Sweden
(Received 22 February 2013; revised manuscript received 17 April 2013; published 14 May 2013)

Recent experimental progress in coupling nanoscale conductors to superconducting microwave cavities has opened up for transport investigations of the deep quantum limit of light-matter interactions, with tunneling electrons strongly coupled to individual cavity photons. We have investigated theoretically the most basic cavity-conductor system with strong, single photon induced nonlocal transport effects: two spatially separated double quantum dots (DQDs) resonantly coupled to the fundamental cavity mode. The system, described by a generalized Tavis-Cummings model, is investigated within a quantum master equation formalism, allowing us to account for both the electronic transport properties through the DQDs as well as the coherent, nonequilibrium cavity photon state. We find sizable nonlocally induced current and current cross-correlations mediated by individual photons. From a full statistical description of the electron transport we further reveal a dynamical channel blockade in one DQD lifted by photon emission due to tunneling through the other DQD. Moreover, large entanglement between the orbital states of electrons in the two DQDs is found for small DQD-lead temperatures.

DOI: 10.1103/PhysRevB.87.195427 PACS number(s): 73.23.Hk, 72.10.Di, 85.25.−j

I. INTRODUCTION

In circuit quantum electrodynamics (QED), the mesoscopic analog of cavity QED, solid state qubits are coupled to superconducting microwave cavities on chip.[1,2] Circuit QED systems combine the appealing properties of high cavity quality factors and strong vacuum microwave fields with low qubit decoherence. This has allowed for experiments in the strong coupling limit with qubit-cavity coupling exceeding the qubits decoherence rates. The strong cavity-qubit coupling together with fast, coherent manipulation of the qubits has lead to an astonishing development in the areas of quantum information processing[3–7] and microwave quantum optics with superconducting circuits.[8–14] Moreover, circuit QED architectures have a large potential for simulations of strongly interacting many-body systems[15] and tests of fundamental quantum physical effects.[16–18]

The rapid development in circuit QED triggered investigations on nanoscale qubits and conductors coupled to microwave cavities or resonators.[19–42] Particularly interesting are recent experiments on few-level quantum dots coherently coupled to microwave cavities.[30,31,37,39–43] These experiments open up for transport investigations of light-matter interactions in the deep quantum regime: single electrons interacting strongly and coherently with individual microwave photons. The large versatility of microwave photon state properties,[17,44,45] together with the well established controllability of quantum dot levels provide a broad scope for fundamentally important experiments.

A key feature of conductor-cavity systems is the possibility to coherently couple electrons in conductors separated up to centimeters.[42] This puts in prospect entangling macroscopically separated transport electrons, of importance for nanoscale quantum information processing and Bell inequality tests.[46–49] Moreover, this nonlocal feature can be harnessed for efficient heat transfer or refrigeration over large distances.[50,51] A first step towards these goals would be an experimental demonstration of nonlocal, few-photon mediated, electronic transport effects. In the present work we investigate theoretically the simplest possible strongly coupled cavity–quantum dot system where such nonlocal effects can be observed: two double quantum dots (DQDs) coupled to the same transmission line cavity (see Fig. 1). We argue that dot-cavity systems with single-level or metallic dots will, in comparison, display suppressed nonlocal effects.

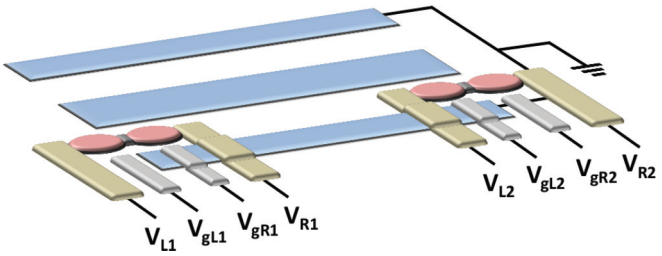

FIG. 1. (Color online) Two DQD-cavity system: Each DQD (pair of red ovals) is coupled to the central conductor of the transmission line cavity (middle blue rectangle), two lead electrodes (gold rectangles) and to two gate electrode potentials (silver rectangles). Here $V_{L(R)i}$ and $V_{gL(R)i}$ denote the left (right) lead and gate electrode potential of DQD i, respectively.

The DQDs are resonantly coupled to the same, fundamental mode of the microwave cavity. This DQD-cavity system constitutes a generalized Tavis-Cummings model,[52,53] with strong hybridization of the DQD electron and microwave photon states. Our investigation is focused on the nonlocal electronic transport properties. For a broad range of parameters, the current-voltage characteristics provide clear signatures of transport electrons exchanging photons. Further, for asymmetric DQD-lead couplings, noise and higher order current fluctuations reveal a dynamical channel blockade in one DQD lifted by single photons emitted by electron tunneling in the second DQD. In addition, we demonstrate the existence of large orbital entanglement between electrons in different DQDs.

We emphasize that the predicted nonlocal effects are direct consequences of the nonequilibrated, transport-induced

photon state. This makes our investigation qualitatively different from earlier transport studies on pairs of two-level systems coupled via thermalized bosons.[54,55] To fully account for the coherent, nonequilibrium properties of the photon state, as well as the electron tunneling through the DQDs, our investigation is carried out within the framework of a quantum master equation (QME). The approach is similar to the ones used to investigate transport through single two-level systems coupled resonantly to a photonic mode in Refs. 24,26, and 36.

The article is organized as follows: In Sec. II A we introduce the model for the closed DQD-cavity system, present its Hamiltonian and discuss the eigenstates and eigenenergies. We further derive, in Sec. II B, a QME for the system when the DQDs are coupled to lead electrodes. In Sec. III the transport properties are investigated in the regime where the temperature of the lead electrodes exceeds the DQD-cavity coupling strength. Focus is put on the nonlocal transport properties, calculating the nonlocal current-voltage characteristics, the current cross-correlations and the full counting statistics. In Sec. IV we turn to the regime where the lead temperature is smaller than the DQD-cavity coupling strength. Transport signatures of coherent electron-photon interaction as well as entanglement between the electrons in the DQDs are investigated. The effect of dephasing and approaches to minimize this effect are discussed in Sec. V.

II. SYSTEM AND METHOD

The system considered is depicted in Fig. 1. Two DQDs, denoted 1 and 2, are inserted near the endpoints of a transmission line cavity. The central conductor is capacitively coupled to the right (left) dot in DQD1(2) (see, e.g., Ref. 39 for a possible experimental realization). One gate and one lead electrode are further coupled to each dot in the DQDs. The leads are assumed to be in thermal equilibrium with a common temperature T and chemical potentials $\mu_{\nu i}$, with $\nu = L, R$ and $i = 1,2$ denoting to which dot the lead is coupled.

Throughout most of the paper we will consider the strong coupling limit. This implies that the DQD-cavity coupling is large compared to the DQD-lead couplings and also dominates over decoherence due to other types of system-environment interaction. Moreover, we will assume the DQD-lead couplings to be much stronger than the interaction with the rest of the system-environment and hence neglect decoherence from the latter. In the last section will we consider the effect of DQD dephasing as well as DQD relaxation and photon loss.

A. Model

The DQDs, forming singly occupied two-level systems, couple linearly to the microwave photons in the cavity. The system Hamiltonian $\hat{H}_S$, describing the DQD-photon interaction as well as the orbital degrees freedom of the DQDs and the direct interaction between the DQD charges, is derived in Appendix A. Below we will take the DQDs to be on resonance with the fundamental mode of the transmission line cavity. Moreover, the cavity characteristic impedance Z_0 is assumed to be much smaller than the resistance quantum $R_Q = h/e^2$, relevant for regular transmission line cavities. Under these conditions the DQD-cavity system will be described by a generalized Tavis-Cummings (TC) Hamiltonian[52]

$$\hat{H}_S = \hbar\omega\hat{a}^\dagger\hat{a} + \sum_i \left[\frac{\hbar\omega}{2}(\hat{d}_{ei}^\dagger\hat{d}_{ei} - \hat{d}_{gi}^\dagger\hat{d}_{gi}) + \hbar g_0(\hat{a}^\dagger\hat{d}_{gi}^\dagger\hat{d}_{ei} + \text{H.c.}) \right]. \quad (1)$$

Here $\hat{d}_{gi}^\dagger$ and $\hat{d}_{ei}^\dagger$ ($\hat{d}_{gi}$ and $\hat{d}_{ei}$) denote the creation (annihilation) operators of the ground and exited, i.e., of the bonding and antibonding, states of DQDi. We have further introduced the photon creation operator $\hat{a}^\dagger$ and the frequency ω of the fundamental mode, and the DQD-cavity coupling strength g_0, for simplicity taken equal for both DQDs. Note that since we have assumed single occupancy of the DQDs, the spin-degree of freedom of the DQDs will only have the effect of renormalizing tunneling rates and is hence neglected in Eq. (1) and below.

The generalized TC Hamiltonian in Eq. (1) has the form of a TC Hamiltonian for both DQDs occupied while it reduces to a Jaynes-Cummings (JC) and a harmonic oscillator (HO) Hamiltonian when one or none of the DQDs are occupied, respectively. It is of key importance for the discussion below to describe the eigenstates in the HO, JC, and TC subspaces of $\hat{H}_S$. We first note that $\hat{H}_S$ commutes with the operator for the number of excitations $\hat{n} = \hat{a}^\dagger\hat{a} + \sum_i \hat{d}_{ei}^\dagger\hat{d}_{ei}$. The eigenstates can then be characterized by the corresponding quantum number n. We express the eigenstates in terms of the DQD-cavity product states $|\xi_1\xi_2 p\rangle$, with DQDi in the state $|\xi_i\rangle$, with $\xi_i = 0, g, e$, and p photons in the cavity mode.

For the HO subspace $\xi_1 = \xi_2 = 0$ and hence the number of excitations is equal to the number of photons, giving the eigenstates $|00n\rangle$. In the JC subspace with DQD1(2) occupied the eigenstate with zero excitations is $|S_1^0 0\rangle = |g00\rangle$ ($|S_2^0 0\rangle = |0g0\rangle$). For states with a finite number of excitations the photon state and the state of the occupied DQD hyridizes. The states, denoted by $|S_i^\pm n\rangle$, are superpositions of product states with n and $n-1$ photons in the mode. For DQD1 occupied they are given by $|S_1^\pm n\rangle = [|g0n\rangle \pm |e0n-1\rangle]/\sqrt{2}$ and for DQD2 occupied we have $|S_2^\pm n\rangle = [|0gn\rangle \pm |0en-1\rangle]/\sqrt{2}$. The eigenbasis in the TC subspace has a similar structure. The state with zero excitations is a product state $|D^0 0\rangle = |gg0\rangle$ and the states with one or more excitations are superpositions of product states with different number of photons. We denote the finite-excitation eigenstates by $|D^\alpha 1\rangle$, with $\alpha = 0, \pm$, for $n = 1$ and $|D^{\beta\gamma} n\rangle$, with and $\beta, \gamma = \pm$, for $n \geqslant 2$ and give their exact forms in Appendix B. The spectra of the HO, JC, and TC Hamiltonians, also given in Appendix B, are shown in Fig. 2. Importantly we see in Fig. 2 that a state with n excitations has an energy $n\hbar\omega + \mathcal{O}(\hbar g_0)$ relative to the energy of the state with zero excitations in its subspace. Moreover the TC (HO) ground state is shifted $-\hbar\omega/2$ ($\hbar\omega/2$) with respect to the JC ground states.

B. Quantum master equation

The leads and their tunnel coupling to the DQDs are described by the Hamiltonians $\hat{H}_L$ and $\hat{H}_T$, respectively. The lead Hamiltonian reads $\hat{H}_L = \sum_{k,\nu,i} \epsilon_k \hat{c}_{k\nu i}^\dagger \hat{c}_{k\nu i}$, with $\hat{c}_{k\nu i}^\dagger$ creating an electron in the state with energy ϵ_k in the lead

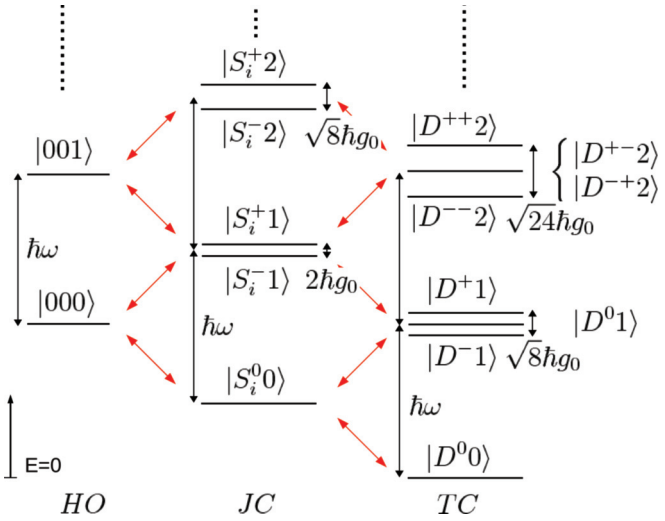

FIG. 2. (Color online) The spectrum of the Hamiltonian in Eq. (1) with the eigenenergies marked by the horizontal black lines. The column to the left shows the spectrum of the HO subspace (both DQDs unoccupied), the middle column shows JC spectrum (DQD1 or DQD2 occupied), and the right column shows the spectrum of the TC subspace (both DQDs occupied). The diagonal red arrows show the allowed transitions due to electron tunneling described by Eq. (3).

connected to dot νi. In the ground-excited basis the tunneling Hamiltonian is given by

$$\hat{H}_T = \sum_{k,i} (t_{Li}\hat{c}^\dagger_{kLi}[-\sin(\theta_i)\hat{d}_{gi} + \cos(\theta_i)\hat{d}_{ei}] + t_{Ri}\hat{c}^\dagger_{kRi}[\cos(\theta_i)\hat{d}_{gi} + \sin(\theta_i)\hat{d}_{ei}] + \text{H.c.}), \quad (2)$$

with $t_{\nu i}$ denoting the energy independent lead-dot tunneling amplitude for dot νi. We have further introduced the DQD mixing angles $\tan(\theta_i) = \pm t_{LRi}/(\sqrt{\omega^2 - t^2_{LRi}} \pm \omega)$, where t_{LRi} denotes the interdot tunneling amplitude of DQDi. The $+(-)$ sign here refers to the energy difference between orbitals of the left and right dots of DQDi being positive (negative).

We assume weak tunnel couplings between the dots and the leads and restrict the investigation to the sequential tunneling regime. Following the standard Born-Markov approximation scheme a quantum master equation (QME) is derived for the time evolution of the reduced density matrix $\hat{\rho}$ of the DQD-cavity system.[56] We point out that the lead-dot tunneling rates $\Gamma_{\nu i} = 2\pi|t_{\nu i}|^2 \sum_k \delta(\epsilon - \epsilon_k)$ must be chosen much smaller than the DQD-cavity coupling strength g_0. This restriction is necessary for the strong coupling condition to hold. Moreover, it allows us to neglect coherences between states with an energy difference $\Delta\epsilon \gtrsim \hbar g_0$, i.e., to perform a secular approximation. Considering for simplicity identical tunnel couplings to the left and right dots in each DQD, i.e., $\Gamma_{Li} = \Gamma_{Ri} = \Gamma_i$, we can write the QME $\frac{d\hat{\rho}}{dt} = \mathcal{L}[\hat{\rho}]$, with the Liouvillian

$$\mathcal{L}[\hat{\rho}] = -\frac{i}{\hbar}[\hat{H}_S, \hat{\rho}] - \sum_{\nu,i}\sum_{\xi=e,g}\int d\epsilon\, d\epsilon' \bar{\Gamma}_{\nu\xi i}(\theta_i) \times [f_{\nu i}(\epsilon)\hat{d}_{\xi i}\delta(\epsilon + \epsilon' - \hat{H}_S)\hat{d}^\dagger_{\xi i}\delta(\epsilon' - \hat{H}_S)\hat{\rho} + \tilde{f}_{\nu i}(\epsilon)\hat{d}^\dagger_{\xi i}\delta(\epsilon + \epsilon' + \hat{H}_S)\hat{d}_{\xi i}\delta(\epsilon' + \hat{H}_S)\hat{\rho} - f_{\nu i}(\epsilon)\delta(\epsilon + \epsilon' - \hat{H}_S)\hat{d}^\dagger_{\xi i}\delta(\epsilon' - \hat{H}_S)\hat{\rho}\hat{d}_{\xi i} - \tilde{f}_{\nu i}(\epsilon)\delta(\epsilon + \epsilon' + \hat{H}_S)\hat{d}_{\xi i}\delta(\epsilon' + \hat{H}_S)\hat{\rho}\hat{d}^\dagger_{\xi i} + \text{H.c.}]. \quad (3)$$

Here $f_{\nu i}(\epsilon) = f(\epsilon - \mu_{\nu i})$ and $\tilde{f}_{\nu i}(\epsilon) = 1 - f(\epsilon - \mu_{\nu i})$, with f denoting the Fermi function. We have further introduced the rates $\bar{\Gamma}_{Lei}(\theta_i) = \bar{\Gamma}_{Rgi}(\theta_i) = \Gamma_i \cos^2(\theta_i)$ and $\bar{\Gamma}_{Lgi}(\theta_i) = \bar{\Gamma}_{Rei}(\theta_i) = \Gamma_i \sin^2(\theta_i)$.

We point out that electron tunneling into or out of the DQDs in the sequential secular regime can be associated with jumps between energy levels in adjacent columns in Fig. 2. This means that the most compelling physical picture will emerge when working in the eigenbasis of $\hat{H}_S$ (see Sec. II A). By evaluating the rates for the different tunneling processes, described by Eq. (3), in this eigenbasis we can draw the following two important conclusions:

(i) The number of excitations of the system can change with 0 or $-(+)1$ when an electron tunnels into (out of) one of the DQDs, as indicated by the red arrows in Fig. 2. The system energy can thus increase or decrease by the energy $\hbar\omega/2 + \mathcal{O}(\hbar g_0)$ in a tunneling event. Consequently, an electron tunneling through one of the DQDs, e.g., from the left lead into the DQD and then out to the right lead, can change the system energy by $0, \pm\hbar\omega + \mathcal{O}(\hbar g_0)$. If a tunneling electron changes the energy with $+(-)\hbar\omega + \mathcal{O}(\hbar g_0)$ a subsequently tunneling electron, in the same or the other DQD, can absorb (emit) this energy. This process, here referred to as the *transport electrons exchanging a photon*, is depicted in Fig. 3.

(ii) The rate for processes where the energy is increased or decreased for an electron tunneling into dot ν in DQDi is proportional to $\bar{\Gamma}_{\nu ei} f_{\nu i}[\hbar\omega/2 + \mathcal{O}(\hbar g_0)]$ and $\bar{\Gamma}_{\nu gi} f_{\nu i}[-\hbar\omega/2 + \mathcal{O}(\hbar g_0)]$, respectively. Similarly, the rates for exciting or deexciting the system when electrons tunnel out of DQDi are given by $\bar{\Gamma}_{\nu gi} \tilde{f}_{\nu i}[-\hbar\omega/2 + \mathcal{O}(\hbar g_0)]$ and $\bar{\Gamma}_{\nu ei} \tilde{f}_{\nu i}[-\hbar\omega/2 + \mathcal{O}(\hbar g_0)]$. Note that the rates for tunneling events in which energy is emitted or absorbed can be controlled by the chemical potentials $\mu_{\nu i}$ and mixing angles θ_i. Note further that for $g_0 = 0$ these rates coincide with the corresponding rates for the DQDs decoupled from the cavity mode, as depicted in Fig. 3.

Based on an analytical solution to the QME (see Appendix C), we can further conclude that a well defined steady-state solution for $\hat{\rho}$ exists for mixing angles $\theta_1, \theta_2 > \pi/4$. For smaller angles and certain bias configurations the photon number can diverge. In Ref. 33, where a single DQD-cavity system was considered, it was shown that DQD mixing angles $\theta < \pi/4$ can lead to population inversion and hence a cavity lasing state.[57–60] Since the focus on this work is the few-photon regime, if not otherwise explicitly stated, we focus on mixing angles $\theta_1, \theta_2 > \pi/4$ below.

III. NONLOCAL TRANSPORT PROPERTIES

The main purpose of this work is to investigate nonlocal transport properties due to exchange of photons between tunneling electrons in different DQDs. This investigation is carried out in the regime $\hbar\omega \gg k_B T \gg \hbar g_0$. The experiments reported in Refs. 30,31, and 39 were performed under these conditions. Moreover, for $k_B T \gg \hbar g_0$ the occupations of

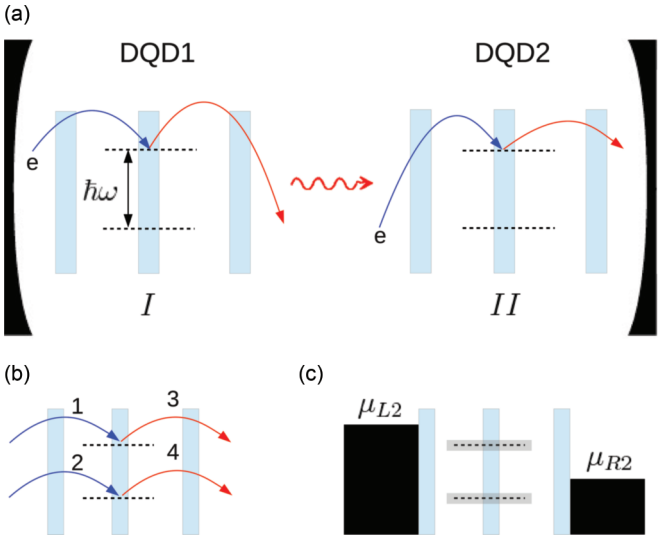

FIG. 3. (Color online) (a) Elementary process in which two transport electrons exchange a photon. In step I an electron tunnels through DQD1, i.e., into (blue arrow) and then out of (red arrow) DQD1, while increasing the system energy by $\hbar\omega$. In step II an electron tunnels through DQD2 and changes the system energy by $-\hbar\omega$. Through steps I and II the two electrons have exchanged a photon (wiggling line) through the cavity. (b) Tunneling processes into and out the ground and excited state of DQDi decoupled from the cavity mode. The rates for the processes 1, 2, 3, and 4 are $\bar{\Gamma}_{Lei} f_{Li}(\hbar\omega/2)$, $\bar{\Gamma}_{Lgi} f_{Li}(-\hbar\omega/2)$, $\bar{\Gamma}_{Rei} \tilde{f}_{Ri}(\hbar\omega/2)$, and $\bar{\Gamma}_{Rgi} \tilde{f}_{Ri}(-\hbar\omega/2)$. (c) Bias configuration of DQD2 considered in Sec. III. The positions of the chemical potentials of the left leads μ_{L2} and μ_{R2} relative to the energies at which electrons tunnel into and out of the DQD are shown. These sets of energies are in an interval $\sim\hbar g_0$ denoted by the grey boxes around the dashed lines.

the leads do not change significantly over the energy scale $\hbar g_0$, i.e., $f_{vi}[\pm\hbar\omega/2 + \mathcal{O}(\hbar g_0)] \approx f_{vi}(\pm\hbar\omega/2)$. Then there are effectively only two energies in the leads at which the electrons can tunnel into and out of the DQDs. This simplifies the expressions for the tunneling rates into and out of the DQDs (see Sec. II B) and allows us to reduce the QME to an ordinary master equation (ME) (see Appendix C). We write this ME $d\mathbf{P}/dt = M\mathbf{P}$, where $\mathbf{P}$ is a vector with the probabilities of eigenstates of $\hat{H}_S$ and M is the matrix with the transition rates between these eigenstates.

For the system to display nonlocal transport effects it is clear that two conditions must be fulfilled: First, transport electrons in different DQDs must exchange photons. Second, for at least one of the DQDs the effective tunneling rate into the empty DQD or out of the occupied DQD must be dependent on the number of excitations in the system or the occupation of the other DQD. The most clear nonlocal effects will thus occur for a state dependence such that transport becomes blocked in one of the DQDs if photons are not emitted by the other. Here we take the DQD2 to be blocked when there are no excitations in the system. This is accomplished by choosing a bias configuration similar to the one depicted in Fig. 3, i.e., such that $f_{L2}(-\hbar\omega/2) = 1$, $f_{L2}(\hbar\omega/2) = 1$, $f_{R2}(-\hbar\omega/2) = 1$, $f_{R2}(\hbar\omega/2) = 0$.

A. Current

We first consider the currents in the DQDs as a function of the bias voltage V_1 across DQD1. The current I_i through DQDi is determined by the populations of the eigenstates of the system and the effective tunneling rates between the DQD and its right lead. The currents $I_1(V_1)$ and $I_2(V_1)$ are plotted for symmetric bias, $\mu_{L1} = -\mu_{R1} = eV_1/2$, and $\theta_1 = \theta_2 = \pi/3$ in Fig. 4. The key feature of both current-voltage characteristics is a thermally broadened onset at $eV_1 = \hbar\omega$. In DQD1 the onset occurs when the energies at which the electron can tunnel into and out of the DQD enter the bias window. The electron tunneling through DQD1 will further excite the system to states where tunneling out of DQD2 becomes possible. Hence the onset of the current I_2 occurs at the same bias voltage V_1. In the limits $\Gamma_1/\Gamma_2 \ll 1$ and $\Gamma_1/\Gamma_2 \gg 1$ the solution to the ME, and hence the currents, can be obtained analytically (see Appendix C). Focusing on the nonlocally induced current $I_2(V_1)$, for symmetric bias and $eV_1 \gg k_BT$ we obtain

$$I_2 = \frac{e\Gamma_1\gamma^2}{1+\gamma}, \quad \Gamma_1/\Gamma_2 \ll 1,$$
$$I_2 = \frac{e\Gamma_2\gamma^2}{[1+2\cot^2(\theta_2)](1-2\gamma+2\gamma^2)+\gamma^2}, \quad \Gamma_1/\Gamma_2 \gg 1, \tag{4}$$

where $\gamma = f_{L1}(\hbar\omega/2)\cos^2(\theta_1)$. From these expressions it is clear that the magnitude of the induced current can be made

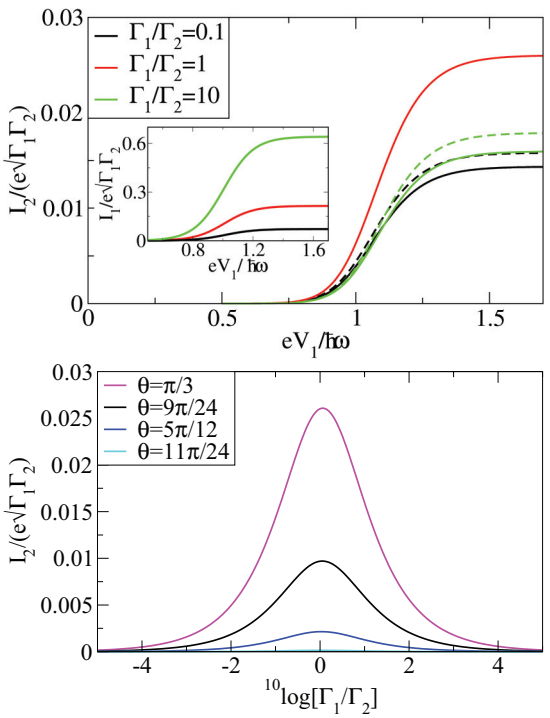

FIG. 4. (Color online) Upper panel: The nonlocally induced current I_2 as a function of $eV_1/\hbar\omega$ for $\theta_1 = \theta_2 = \pi/3$, $k_BT = 0.05\hbar\omega$ and different asymmetry factors Γ_1/Γ_2. The dashed black (green) curve shows the current for $\Gamma_1/\Gamma_2 = 1/10$ (10) obtained from the analytical expression for $\Gamma_1 \ll \Gamma_2$ ($\Gamma_2 \ll \Gamma_1$) in Eq. (4). The inset shows I_1 as a function of $eV_1/\hbar\omega$ for the same asymmetry factors and mixing angles. Lower panel: The current I_2 above the onset voltage against the asymmetry factor Γ_1/Γ_2 for different $\theta = \theta_1 = \theta_2$.

$\sim e\Gamma_1$ and $\sim e\Gamma_2$ in the limits $\Gamma_1/\Gamma_2 \ll 1$ and $\Gamma_1/\Gamma_2 \gg 1$, respectively. From the plot of the high-bias current against the asymmetry factor Γ_1/Γ_2 for $\theta_1 = \theta_2$ in Fig. 4 and from further investigation for $\theta_1 \neq \theta_2$, we find that the nonlocal effect is maximal for $\Gamma_1 \sim \Gamma_2$. We can thus conclude that the nonlocally induced current, qualitatively behaving as $I_2 \sim e\Gamma_1\Gamma_2/(\Gamma_1 + \Gamma_2)$, is considerable for a large range of the parameters Γ_1, Γ_2, θ_1, and θ_2. Note that the expressions in Eq. (4) do not depend on g_0, a consequence of considering the strong coupling regime, $\Gamma_i \ll g_0$, and the temperature limit $\hbar g_0 \ll k_B T$.

To estimate the magnitude of the nonlocally induced current we consider recent single DQD-cavity experiments,[39,41] where fundamental frequencies $\omega/2\pi \sim 10$ GHz and DQD-cavity coupling strengths $g_0/2\pi \sim 50$ MHz were reported. For these parameters strong coupling is achieved for tunneling rates $\Gamma_i \lesssim 50$ MHz giving nonlocally induced currents of the order $I_2 \sim 0.1$ pA. Importantly, currents of this magnitude have been measured in DQD-cavity systems.[39]

To further put the magnitude of the nonlocally induced current in perspective we briefly discuss nonlocal transport properties for the system with the DQDs replaced by single-level or metallic dots. As follows from our Ref. 34, the MEs describing the evolution of these systems are explicitly dependent on the parameter Z_0/R_Q, typically much smaller than unity for regular transmission lines. Importantly, the MEs show that the effective tunneling rate into an empty dot or out of an occupied dot is independent on the system state to zero order in Z_0/R_Q. It thus follows that the nonlocally induced current will be proportional to Z_0/R_Q, to first nonvanishing order. In a single-level or metallic dot-cavity system the nonlocally induced current will thus, in comparison with the current in a DQD-cavity system, be suppressed.

B. Current correlations

We have now established that photon exchange between transport electrons in the spatially separated DQDs can result in a nonlocal current. As the next natural step, we investigate the mechanism behind this exchange. To this aim we consider the low-frequency correlations S_{ij} between the currents in DQDi and DQDj. Current correlations are known to provide information about, e.g., the effective charge, interactions, and statistical properties of the charge carriers.[61] The correlations S_{ij} can formally be obtained from a number-resolved version of the ME (see Appendix D). Focusing first on the cross-correlations S_{12} we plot in Fig. 5 the cross-correlation Fano factor $F_{12} = S_{12}/(e\sqrt{I_1 I_2})$ against the bias voltage V_1 for different asymmetry factors. Similar to the normalized currents I_1 and I_2, the cross-correlations have an onset at $eV_1 = \hbar\omega$. However, in contrast to the current I_2 (but similar to I_1) the cross-correlations have a strong dependence on the asymmetry factor Γ_1/Γ_2. This can be seen by considering the limits $\Gamma_1/\Gamma_2 \ll 1$ and $\Gamma_1/\Gamma_2 \gg 1$ where analytical expressions can be obtained. Above the onset voltage we get

$$F_{12} = \frac{\cos(\theta_1)[1+\cos^4(\theta_1)]}{[1+\cos^2(\theta_1)]^2}, \quad \Gamma_1/\Gamma_2 \ll 1,$$
$$F_{12} = \mathcal{O}(\sqrt{\Gamma_2/\Gamma_1}), \quad \Gamma_2/\Gamma_1 \ll 1. \tag{5}$$

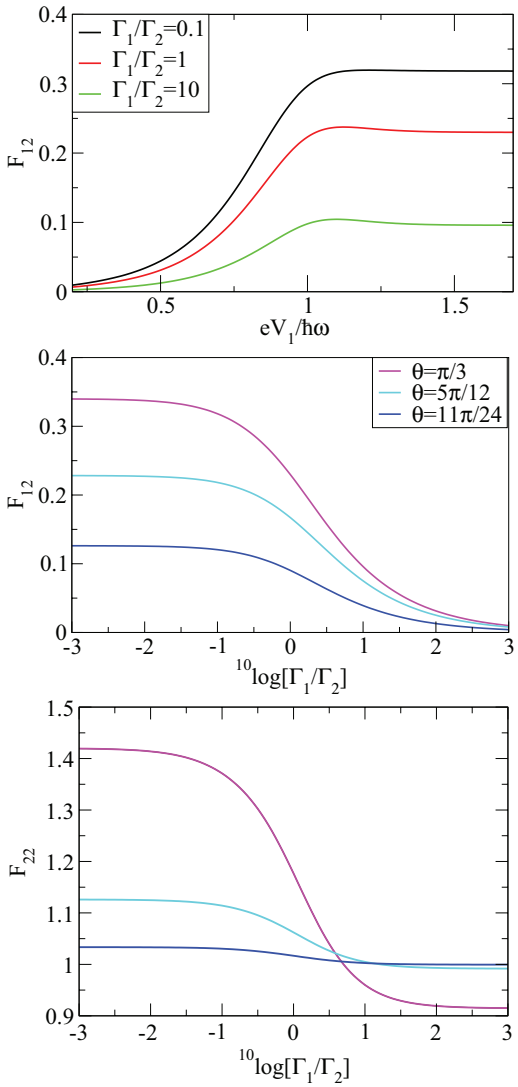

FIG. 5. (Color online) Upper panel: Cross-correlation Fano factor $F_{12} = S_{12}/(e\sqrt{I_1 I_2})$ as a function of eV_1 for different asymmetry factors Γ_1/Γ_2 for mixing angles $\theta_1 = \theta_2 = \pi/3$ and temperature $k_B T = 0.05\hbar\omega$. Middle panel: Cross-correlation Fano factor above onset as a function of asymmetry parameter Γ_1/Γ_2 for $\theta_1 = \theta_2 = \theta$ and $k_B T \ll \hbar\omega$. Lower panel: Auto-correlation Fano factors $F_{22} = S_{22}/I_2$ above onset as a function of asymmetry parameter for mixing angles $\theta_1 = \theta_2 = \theta$ and $k_B T \ll \hbar\omega$.

From these expressions we see that the currents in DQD1 and DQD2 are manifestly positively correlated, $F_{12} > 0$ [$\cos(\theta_1) > 0$], for $\Gamma_1/\Gamma_2 \ll 1$. The correlations are also strong, $F_{12} \sim 1$. In contrast, for $\Gamma_1/\Gamma_2 \gg 1$, the currents are essentially uncorrelated. The crossover between the two regimes is shown in Fig. 5 for $\theta_1 = \theta_2$. The strong, positive correlations appearing for $\Gamma_1 \lesssim \Gamma_2$ clearly show that tunneling through DQD2 is triggered by tunneling through DQD1. The qualitatively different system behavior in the limits $\Gamma_1/\Gamma_2 \ll 1$ and $\Gamma_1/\Gamma_2 \gg 1$, respectively is also manifested in the auto-correlations S_{22}. In Fig. 5 we see that the autocorrelation Fano factor $F_{22} = S_{22}/(eI_2)$ above onset goes from a sub-Poissonian value, $F_{22} < 1$, to a super-Poissonian value, $F_{22} > 1$, as the asymmetry factor Γ_2/Γ_1 is decreased from infinity to zero.

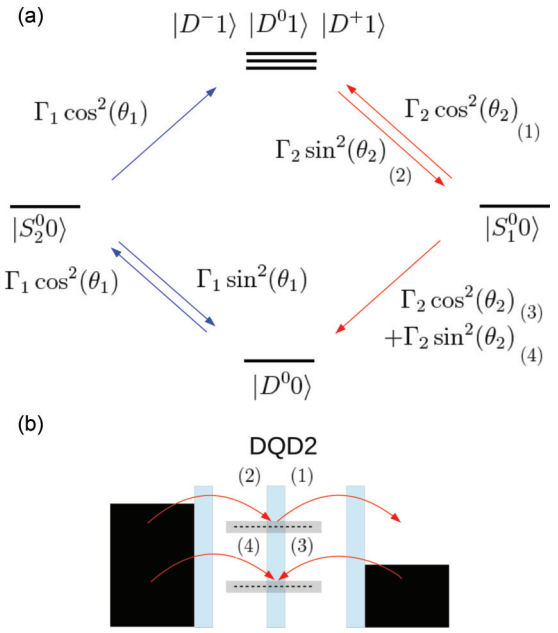

FIG. 6. (Color online) (a) Schematic of processes in ME $d\mathbf{P}/dt = M\mathbf{P}$ contributing to tranbsport quantities to first order in the asymmetry parameter Γ_1/Γ_2. The tunneling processes in DQD1 (slow processes) are marked by blue arrows and the tunneling processes in DQD2 (fast processes) are marked by red arrows. (b) Tunneling processes in DQD2. Process (1) and (2) describe the tunneling into and out of the DQD as the system goes back-and forth between $|S_1^0 0\rangle$ and $\{|D^\alpha 1\rangle\}$. Processes (3) and (4) describe the tunneling processes where the system relaxed from $|S_1^0 0\rangle$ to $|D^0 0\rangle$.

This describes a transition from antibunching to bunching behavior of the transport electrons.[61]

To connect these findings to the properties of the photon exchange we first perform a careful investigation of the ME in the limit $\Gamma_1 \ll \Gamma_2$. The processes contributing to transport quantities to leading order in the asymmetry parameter Γ_1/Γ_2 are depicted in Fig. 6. From this scheme it is apparent that the states $|D^0 0\rangle$ and $|S_2^0 0\rangle$ will have occupations $\mathcal{O}(1)$, while the other states have occupation $\mathcal{O}(\Gamma_1/\Gamma_2)$. The system will thus spend most of its time in the states $|D^0 0\rangle$ and $|S_2^0 0\rangle$ and will occasionally be excited out of this subspace by a tunneling event in DQD1, from the state $|S_2^0 0\rangle$ to any of the states $\{|D^\alpha 1\rangle\}$. The system can from here go back and forth between $\{|D^\alpha 1\rangle\}$ and $|S_2^0 0\rangle$ an arbitrary number of times before relaxing to $|D^0 0\rangle$. This will occur on a time-scale $\sim 1/\Gamma_2$. Each tunneling event in DQD1 which excites the system to $\{|D^\alpha 1\rangle\}$ will hence be followed by one or more tunneling events in DQD2 during a short time window $\sim 1/\Gamma_2$. The electrons in DQD2 are thus transported in cascades induced by randomly occurring tunneling events in DQD1 with separation $1/\Gamma_1 \gg 1/\Gamma_2$. This mechanism, commonly referred to as dynamical channel blockade,[62,63] explains both the positive cross-correlations, $S_{12} > 0$, and the bunching of electrons in DQD2, $F_{22} > 1$. Importantly, each cascade in DQD2 is initiated by the emission of a single photon due to an electron tunneling through DQD1.

To further discuss photon exchange in the opposite limit $\Gamma_1 \gg \Gamma_2$ we note that many tunneling events in DQD1 occur in between each tunneling event in DQD2. As a consequence the distribution of excitations is entirely determined by the tunneling in DQD1 (see Appendix C). This means that the steady-state distribution of excitations is restored in between each (photon-assisted) tunneling event out of DQD2. The tunneling events out of DQD2 are thus, in clear contrast to the case in the opposite limit $\Gamma_1 \ll \Gamma_2$, not triggered by photon emission in single tunneling events in DQD1. This explains the suppression of the current cross-correlations as well as the sub-Poissonian auto-correlations in DQD2. In conclusion our investigation supports the physical picture where individual tunneling electrons in DQD1 and DQD2 exchange single photons for $\Gamma_1 \ll \Gamma_2$ (but not for $\Gamma_1 \gg \Gamma_2$) and that this process is clearly manifested in the current correlations.

C. Full counting statistics

To obtain a complete picture of the elementary processes of the charge transport for $\Gamma_1 \ll \Gamma_2$ we consider the full transport statistics. The statistics is most clearly visualized via the cumulant generating function (CGF) $\mathcal{F}$ which can be obtained analytically above onset (see Appendix D) and is given by

$$\begin{aligned}\mathcal{F}(\chi_1,\chi_2) &= -\frac{\Gamma_1}{2}(1+\cos^2(\theta_1) \\ &\quad -\sqrt{\sin^4(\theta_1)+4\cos^2(\theta_1)e^{i\chi_1}[\sin^2(\theta_1)+\cos^2(\theta_1)y]}), \\ y &= [\cos^2(\theta_2)+\sin^2(\theta_2)e^{i\chi_2}]\sum_{n=0}\frac{z^n}{z_0}e^{in\chi_2}. \end{aligned} \quad (6)$$

Here $z = \cos^2(\theta_2)/[1+\cos^2(\theta_2)]$, $z_0 = 1+\cos^2(\theta_2)$, and χ_i is the counting field for charge transfer in DQDi. To interpret the CGF we first consider the case when the charge transfer through DQD2 is not monitored, i.e., $\chi_2 = 0$. Then $y = 1$ and the CGF reduces to the well known result[64] for a single level dot with tunneling rates Γ_1 and $\Gamma_1\cos^2(\theta_1)$ into and out of the dot, respectively. For $\chi_2 \neq 0$, it is clear from the term $\sin^2(\theta_1) + \cos^2(\theta_1)y$ that tunneling events into DQD1 are of two kinds. First, for events corresponding to the transition $|S_2^0\rangle \to |D^0 0\rangle$, occurring with a rate $\propto \sin^2(\theta_1)$, there is no tunneling in DQD2. The second type of events, corresponding to transitions $|S_2^0 0\rangle \to \{|D^\alpha 1\rangle\}$ and occurring with a rate $\propto \cos^2(\theta_1)$, trigger tunneling in DQD2. This tunneling takes place as the system goes back to $|D^0 0\rangle$ and is described by the function $y = y(\chi_2)$.

The different terms in y are given by the probabilities for all possible processes taking the system from $\{|D^\alpha 1\rangle\}$ to $|D^0 0\rangle$, weighted with counting field factors describing the respective charge transfer through DQD2. Common for all processes is that they start with the transition $\{|D^\alpha 1\rangle\} \to |S_1^0 0\rangle$ and end with $|S_1^0 0\rangle \to |D^0 0\rangle$. These two transitions give rise to the prefactor $\cos^2(\theta_2) + \sin^2(\theta_2)e^{i\chi_2} = e^{i\chi_2}[\cos^2(\theta_2)e^{-i\chi_2} + \sin^2(\theta_2)]$, with the $e^{i\chi_2}$ from the starting transition and $\cos^2(\theta_2)e^{-i\chi_2} + \sin^2(\theta_2)$ from the ending transition. As shown in Fig. 6, the ending transition can occur via tunneling from the left lead of DQD2 [probability $\sin^2(\theta_1)$, no counting field factor] or back from the right lead of DQD2 [probability $\cos^2(\theta_1)$, counting field factor $e^{-i\chi_2}$]. The sum term in y, running from zero to infinity, describes all possible back-and-forth transitions $|S_1^0 0\rangle \to \{|D^\alpha 1\rangle\} \to |S_1^0 0\rangle$ the system can perform, between the starting and ending transitions (see Fig. 6). The nth term in the sum thus corresponds to

n transitions and hence n electrons being transferred across DQD2. This interpretation comes naturally when noting that z^n/z_0 is the probability of returning to the state $|D^\alpha 1\rangle n$ times. The structure of the CGF, and in particular y, clearly shows that that electrons in DQD2 are transported in cascades and that these cascades are triggered by single photons emitted by electrons tunneling through DQD1.

IV. SPECTRAL FINE STRUCTURE AND ENTANGLEMENT

It is interesting to investigate what qualitatively new physical effects come into play in the regime where the thermal broadening in the leads is much smaller than the DQD-cavity coupling strength, i.e., $k_BT \ll \hbar g_0$. In this regime the ME description used in the previous section is no longer valid and we need to consider the full QME of Eq. (3).

A. Transport properties

We first demonstrate that the structure on the scale $\sim\hbar g_0$ in the spectrum of the generalized TC Hamiltonian appear in the transport properties of the system for $k_BT \lesssim \hbar g_0$. This fine structure, a manifestation of coherent electron-photon interaction, appear already in the average current and we therefore focus on this quantity. Moreover, we consider the simplest possible parameter regime by taking DQDs with identical mixing angles $\theta_1 = \theta_2 = \theta$, lead-DQD tunneling rates $\Gamma_1 = \Gamma_2 = \Gamma$, and with left (right) leads having the same chemical potential, i.e., $\mu_{v1} = \mu_{v2} = \mu_v$. This will give the same current $I = I_1 = I_2$ in DQD1 and DQD2. This current I is readily obtained from a numerical solution of Eq. (3) (see Appendix D for details). In Fig. 7 we plot $I(V)$ for symmetric bias voltage $\mu_L = -\mu_R = eV/2$ and $\theta = \pi/3$ for temperatures ranging from $k_BT \sim \hbar g_0$ down to $k_BT \ll \hbar g_0$. We clearly see how the single step onset at $eV = \hbar\omega$ is split up into several smaller steps, spaced $\sim\hbar g_0$ as the temperature is decreased. These steps can directly be attributed to the structure of the spectrum of the generalized TC Hamiltonian. They are a consequence of eigenstates with energy splittings $\sim\hbar g_0$ becoming populated at different bias voltages. It is here interesting to note that signatures of the JC spectrum were found in the frequency-dependent current auto-correlations in the transport through a system with only one DQD coupled to the cavity mode.[25]

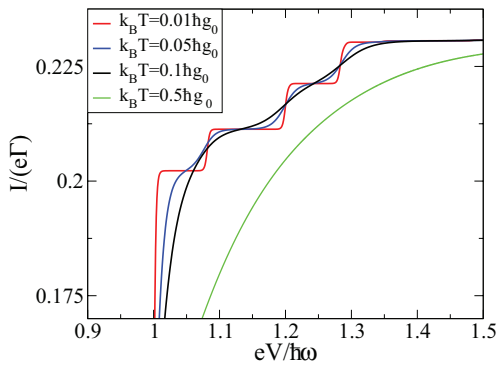

FIG. 7. (Color online) The current $I = I_1 = I_2$ through the DQDs as a function of voltage above onset for $\theta = \pi/3$, $g_0 = 0.1\omega$, and different temperatures.

B. Transport-induced entanglement

A natural question to ask when considering two coupled, spatially separated DQDs is to what extent their orbital degrees of freedom become entangled by the exchange of cavity photons. The object of interest, describing the properties of the electronic state with one electron in each DQD, is the reduced two-particle density matrix $\hat{\rho}_r$. The reduced density matrix, of dimension 4×4, is formally obtained by first projecting the total system density matrix $\hat{\rho}$ onto the TC subspace and then tracing out the photonic degrees of freedom. As follows from the structure of Eq. (3) and the TC eigenstates (Appendix B), the reduced density matrix can be written as a sum of the four diagonal components in the singlet-triplet basis,

$$\hat{\rho}_r = \rho_g|gg\rangle\langle gg| + \rho_e|ee\rangle\langle ee| + \rho_S|\mathcal{S}\rangle\langle\mathcal{S}| + \rho_T|\mathcal{T}\rangle\langle\mathcal{T}|, \tag{7}$$

where $|\mathcal{S}(\mathcal{T})\rangle = (|eg\rangle - (+)\,|ge\rangle)/\sqrt{2}$. The entanglement of $\hat{\rho}_r$ is conveniently quantified via the concurrence,[65] ranging from 1 for a maximally entangled state to 0 for a nonentangled, separable state. For a density matrix of the form in Eq. (7) the concurrence $C(\hat{\rho}_r)$ takes on the simple form

$$C = \max\{|\rho_S - \rho_T| - 2\sqrt{\rho_e\rho_g}, 0\}. \tag{8}$$

To determine if entanglement can be induced by photon exchange we first consider the scheme in Fig. 8, displaying the lowest energy states with the TC subspace well resolved. By noting that the lowest excited TC states $|D^\alpha 1\rangle$ are written $|D^0 1\rangle = |\mathcal{S}0\rangle$ and $|D^\pm 1\rangle = (1/\sqrt{2})(|gg1\rangle \pm |\mathcal{T}0\rangle)$ it is clear that a selective population of any of the $|D^\alpha 1\rangle$ states would give an electronic state with a large singlet ($\mathcal{S}$) or entangled triplet ($\mathcal{T}$) component. To demonstrate such a selective population we choose bias voltages V_i and dot-level positions such that the chemical potentials μ_{iL} and μ_{iR} obey the relations

$$\begin{aligned} \frac{\hbar\omega}{2} - \sqrt{2}\hbar g_0 < \mu_{Li} < \frac{\hbar\omega}{2} - \hbar g_0, \\ -\frac{\hbar\omega}{2} > \mu_{Ri} > -\frac{\hbar\omega}{2} - (\sqrt{2}-1)\hbar g_0. \end{aligned} \tag{9}$$

For $k_BT \ll \hbar g_0$ then only $|D^-1\rangle$ of the excited TC states becomes populated.

For the chosen parameters, as seen in Fig. 8, only five states of the generalized TC model contribute to transport. For this case the QME can be solved exactly. Importantly, the steady-state solution gives a reduced two-particle density

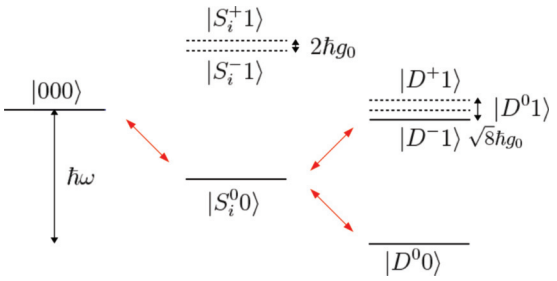

FIG. 8. (Color online) Scheme of the lowest energy levels in the generalized TC Hamiltonian. The red arrows show the active transitions for $k_BT \ll \hbar g_0$ and for a bias configuration such that the chemical potentials satisfy the conditions in Eq. (9).

matrix $\hat{\rho}_r$ with only ρ_g and ρ_T nonzero. As is clear from Eq. (8) the resulting concurrence is finite. For a symmetric parameter setting, i.e., for $\theta_1 = \theta_2 = \theta$, $\Gamma_1 = \Gamma_2 = \Gamma$, and $\mu_{v1} = \mu_{v2} = \mu_v$ this concurrence is given by

$$C = \frac{\cos^4(\theta)}{2[\cos^4(\theta) + \sin^4(\theta)]}, \tag{10}$$

showing that the concurrence can reach up to $C = 1/2$ for $\theta \ll 1$. We stress that for the chosen parameters there is no bound on θ in order to have a well defined solution to the QME.

Having confirmed the existence of large entanglement $C \lesssim 1/2$, we consider the effect of finite temperature and modified bias voltage $V = V_1 = V_2$. Solving numerically the QME, the resulting concurrence $C(V)$ is plotted in Fig. 9 for different temperatures. For low temperatures $k_B T \ll \hbar g_0$ the entanglement has an onset when $|D^- 1\rangle$ is populated, with the concurrence given by Eq. (10). Increasing the voltage further, $|D^0 1\rangle$ is populated as well, decreasing the concurrence due to the finite probability for both entangled triplet, ρ_T and singlet, ρ_S, electronic states, clear from Eq. (8). For even larger bias all TC states $|D^\alpha 1\rangle$ have finite population and the entanglement disappears. From Fig. 9 it is also clear that increasing the temperature smears the $C(V)$ curve and successively suppresses the entanglement, reaching a separable state at $k_B T \approx \hbar g_0/2$.

We can thus conclude that both in the high-bias and high-temperature regimes, where the system can be described by a ME, the entanglement is zero. To clarify the generality of this observation we investigated the concurrence in all regimes where we could solve the ME analytically (see Appendix C). In these regimes we could formally prove the absence of entanglement. Moreover we considered the concurrence obtained numerically for a broad range of other system parameters in the ME regime but did not find any entanglement. We thus conclude that it is highly probable that for $\Gamma_i \ll g_0$ electrons in the two DQDs can only be entangled for temperatures $k_B T \ll \hbar g_0$, in biasing regimes where TC states with the same number of excitations are selectively populated.

We stress that our investigation mainly aims at demonstrating the existence of entanglement. We do not analyze how or even if it can be detected by transport measurements. A detailed comparison of our results to the ones of existing proposals in various coupled DQD systems, see e.g., Refs. 55 and 66–69, is also beyond the scope of the present article.

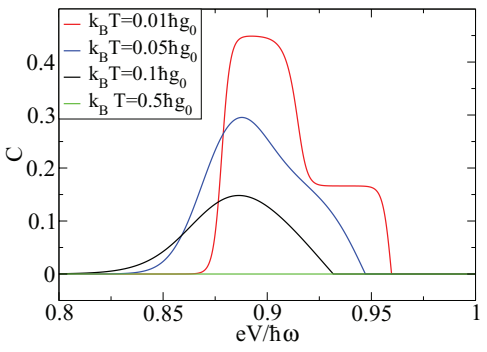

FIG. 9. (Color online) Concurrence C as a function of bias voltage for different temperatures for $g_0 = 0.1\omega$, $\mu_L + \mu_R = -0.12\hbar\omega$, and $\theta_1 = \theta_2 = \pi/6$.

V. DEPHASING AND RELAXATION EFFECTS

So far we have neglected dephasing and relaxation effects in the DQDs as well as loss of cavity photons. From the recent single DQD experiments[39,41] it is clear that the dephasing rate Γ_D is much larger than the rates Γ_R and κ for relaxation and cavity loss, respectively. We thus focus on the effect of dephasing on the results presented above.

Dephasing can qualitatively be accounted for by adding a term[70]

$$\mathcal{L}_D[\hat{\rho}] = \frac{\Gamma_D}{2} \sum_{i=1,2} [2\hat{L}_i \hat{\rho} \hat{L}_i^\dagger - \hat{L}_i^\dagger \hat{L}_i \hat{\rho} - \hat{\rho} \hat{L}_i^\dagger \hat{L}_i] \tag{11}$$

to the Liouvillian in Eq. (3). Here $\hat{L}_i = \hat{d}_{ei}^\dagger \hat{d}_{ei} - \hat{d}_{gi}^\dagger \hat{d}_{gi}$ and the dephasing is taken to be independent, with the same rate Γ_D, for the two DQDs. An investigation of dephasing in all parameter regimes is beyond the scope of the present article. However, we stress that for strong dephasing, $\Gamma_D \gg g_0$, coherent superpositions between excited and ground states in the DQDs are suppressed. The steady-state solution of Eqs. (3) and (11) is diagonal in the basis of the DQD-cavity product states $|\xi_1 \xi_2 p\rangle$, with $\xi_i = 0, g, e$, and p the number of photons. As a consequence, electrons and photons are decoupled and the nonlocal transport effects as well as the DQD entanglement appearing in the regime $\hbar g_0 \gg k_B T$ are suppressed.

Importantly, in both single DQD experiments[39,41] the dephasing is found to be strong, with $\Gamma_D \sim 1$ GHz, substantially larger than the coupling strength $g_0/2\pi \sim 50$ MHz. It is thus necessary to consider ways to increase g_0 and/or suppress Γ_D, in order to approach the strong coupling limit $g_0 \gg \Gamma_D$ where the nonlocal effects discussed above are fully developed. First and foremost, the coupling g_0 can be increased substantially by increasing the fundamental frequency ($g_0 \propto \omega$), simply by making a shorter cavity. Importantly, since we consider an isolated cavity, ω is not limited by requirements of an external microwave circuitry. The limit is instead set by the energy gap of the superconducting cavity material, of the order of hundreds of GHz for large gap superconductors, e.g., Nb ($\omega/2\pi \approx 10$ GHz in Refs. 39 and 41). Second, unconventional transmission line cavities, with a central conductor consisting of, e.g., Josephson junctions or superconducting quantum interference device (SQUIDS),[71–73] can have characteristic impedances $Z_0 \sim 1$ kΩ. This gives coupling strengths $g_0 \sim 0.1\omega$, one order of magnitude larger than for conventional transmission lines. Third, since Refs. 39 and 41 are the first experiments on DQDs in cavities, there is probably room for optimizing the circuit design, further suppressing the dephasing. Taken together, the strong coupling limit of our proposal is arguably within reach experimentally. Moreover, the relaxation rate in Ref. 39 was estimated to be $\Gamma_R \sim 100$ MHz, one order of magnitude smaller than the dephasing rate. Hence, in the strong coupling limit $g_0 \gg \Gamma_D$, relaxation is expected to be negligible. In addition, the cavity loss rate κ in Refs. 39 and 41 was already much smaller than g_0, suggesting that cavity loss can safely be neglected.

VI. CONCLUSION

In conclusion we have theoretically investigated the nonlocal transport properties of a DQD-cavity system. We have found that the photons emitted by electrons tunneling in one DQD can assist transport of electrons through the other DQD, giving a strong nonlocally induced current and large cross-correlations between currents in the two DQDs. Moreover, in the low-temperature regime, $k_BT \ll \hbar g_0$, we have demonstrated that signatures of the TC spectrum will appear in the I-V characterstics and that the orbital degrees of freedom of electrons in the two DQDs can become entangled. Importantly, our work provides a theoretical framework for investigations of nonlocal electronic transport properties in cavity-coupled nanoscale conductors. The analysis can readily be modified to study transport through other nanoscopic two-level systems coupled to cavities, e.g., superconducting single electron transistors[21,24] and spin qubits.[22,36,41,74]

Note added in proof. Recently, two eprints[83,84] on transport through two DQDs coupled via a cavity mode appeared.

ACKNOWLEDGMENTS

We thank Seigo Tarucha, Per Delsing, Daniel Karlsson, Olov Karlström, and Cecilia Jarlskog for fruitful discussions and input. We would further like to thank Christian Flindt, Björn Sothmann, Tineke van der Berg, and Martin Leijsne for constructive comments on an earlier version of the manuscript. We also acknowledge discussion with Deborah Contreras-Pulido on a manuscript in preparation on a closely related problem. The work was supported by the Swedish VR.

APPENDIX A

We here derive the Hamiltonian for the DQD-transmission line cavity system. The first step is to describe the DQDs within the standard[75] constant-interaction model. Then only the excess dot charges will interact capacitively with the cavity. This means that the total Hamiltonian of the system, $\hat{H}_S$, becomes the sum of the Hamiltonian for the orbital states of the DQDs, $\hat{H}_O$, and the Hamiltonian for the cavity, the dot charges, and their interactions, $\hat{H}_C$. For the orbital part $\hat{H}_O$ we consider DQDs formed by two tunnel coupled quantum dots with a single active spin-degenerate level in each dot. The orbital part of the Hamiltonian, in the localized basis of the DQDs, then has the form

$$\hat{H}_O = \sum_{i=1,2} \frac{\Delta_i}{2}(\hat{d}^\dagger_{Li}\hat{d}_{Li} - \hat{d}^\dagger_{Ri}\hat{d}_{Ri}) + t_{LRi}(\hat{d}^\dagger_{Li}\hat{d}_{Ri} + \hat{d}^\dagger_{Ri}\hat{d}_{Li}) \tag{A1}$$

with Δ_i being the energy difference between the bare energies of the orbitals in the left and right dots of DQDi. We recall that t_{LRi} denotes the interdot tunneling amplitude of DQDi and note that the creations operators $\hat{d}^\dagger_{Li}$,$\hat{d}^\dagger_{Ri}$ are related to the eigenbasis creation operators creation operators according to

$$\begin{aligned}\hat{d}^\dagger_{Li} &= -\sin(\theta_i)\hat{d}^\dagger_{gi} + \cos(\theta_i)\hat{d}^\dagger_{ei},\\ \hat{d}^\dagger_{Ri} &= \cos(\theta_i)\hat{d}^\dagger_{gi} + \sin(\theta_i)\hat{d}^\dagger_{ei}.\end{aligned} \tag{A2}$$

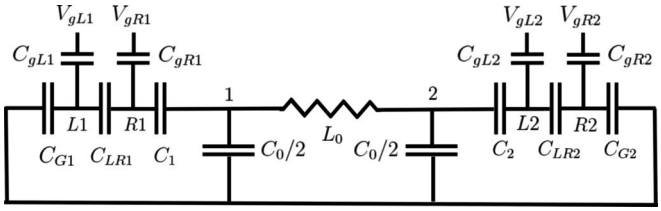

FIG. 10. Diagram of the circuit describing the transmission line cavity, the dot charges and their interactions. In DQD1 (DQD2) the right (left) dot is coupled capacitively to the central conductor of the transmission line, modeled by an LC circuit and to two gate electrodes. The nodes vi correspond to the dots while node 1 and 2 correspond to the endpoints of the transmission line.

The Hamiltonian $\hat{H}_C$ is derived within the framework of circuit QED. Following the procedure of Refs. 34,76, and 77 we start from the classical Lagrangian of a circuit representation of the system, including the capacitances of the dots. The transmission line is modeled by a single LC circuit. This will describe the physics of one finite-frequency mode (the fundamental mode)[78] and the zero-frequency mode. The circuit diagram is shown in Fig. 10, where C_{Gi}, C_{gvi}, C_{LRi}, C_i, and V_{gvi} denote the capacitances and gate voltages of DQDi, and L_0, C_0 are the total inductance and total capacitance to ground of the central conductor.

The Lagrangian of the circuit is given by

$$\begin{aligned}\mathscr{L} = \sum_{i=1,2}\Bigg(&\frac{C_i(\dot{\phi}_i - \delta_{i1}\dot{\phi}_{Ri} - \delta_{i2}\dot{\phi}_{Li})^2}{2} + \frac{C_0\dot{\phi}_i^2}{4}\\ &+ \frac{C_{LRi}(\dot{\phi}_{Li} - \dot{\phi}_{Ri})^2}{2} + \frac{\sum_\nu C_{g\nu i}(\dot{\phi}_{\nu i} - V_{g\nu i})^2}{2}\Bigg)\\ &+ \frac{C_{G1}\dot{\phi}^2_{L1} + C_{G2}\dot{\phi}^2_{R2}}{2} - \frac{(\phi_1 - \phi_2)^2}{2L_0},\end{aligned} \tag{A3}$$

where $\phi_{\nu i}$ and ϕ_i denote the phases of nodes νi and i, respectively (see Fig. 10). The zero- and finite-frequency normal modes, describing the electrostatics and electrodynamics of the circuit, respectively, are obtained from the Euler-Lagrange equations. By rewriting the Lagrangian in terms of these normal modes, performing a Legendre transformation and a canonical quantization of the fundamental mode, a quantum Hamiltonian, $\hat{H}_C$, is obtained. By further writing the excess charges of the dots as $e(\hat{d}^\dagger_{\nu i}\hat{d}_{\nu i} - n_{g\nu i})$, where $n_{g\nu i}$ denotes the gate-induced charges, we get $\hat{H}_C = \hat{H}_I + \hat{H}_{DI0} + \hat{H}_{DI1}$, with

$$\begin{aligned}\hat{H}_I &= \hbar\omega\hat{a}^\dagger\hat{a} + \sum_{\nu i}\Bigg[\frac{e^2(\hat{d}^\dagger_{\nu i}\hat{d}_{\nu i} - n_{g\nu i})^2}{2\tilde{C}_{\nu i}}\\ &\qquad + \lambda_{\nu i}(\hat{a}^\dagger + \hat{a})(\hat{d}^\dagger_{\nu i}\hat{d}_{\nu i} - n_{g\nu i})\Bigg],\\ \hat{H}_{DI0} &= \sum_{\nu\mu} U_{\nu 1\mu 2}(\hat{d}^\dagger_{\nu 1}\hat{d}_{\nu 1} - n_{g\nu 1})(\hat{d}^\dagger_{\mu 2}\hat{d}_{\mu 2} - n_{g\mu 2}),\\ \hat{H}_{DI1} &= \sum_{\nu\mu}\frac{\lambda_{\nu 1}\lambda_{\mu 2}}{2\hbar\omega}(\hat{d}^\dagger_{\nu 1}\hat{d}_{\nu 1} - n_{g\nu 1})(\hat{d}^\dagger_{\mu 2}\hat{d}_{\mu 2} - n_{g\mu 2}),\end{aligned} \tag{A4}$$

In the total Hamiltonian $\hat{H}_S = \hat{H}_C + \hat{H}_O$, the part $\hat{H}_O + \hat{H}_I$ has the standard form for a few-level dot system linearly coupled to a bosonic mode (see, e.g., Ref. 79), with $\tilde{C}_{\nu i}$ and

λ_{vi} denoting the effective self-capacitances of the dots and the coupling strengths between the photons of the fundamental mode and the dot charges, respectively. The part $\hat{H}_{DI0}$ contains cross terms, $\sim \hat{d}^\dagger_{v1}\hat{d}_{v1}\hat{d}^\dagger_{\mu 2}\hat{d}_{\mu 2}$, describing direct nonlocal coupling between the dot charges. The coupling strengths, $U_{v1\mu 2}$, depend parametrically only on the capacitances of the circuit in Fig. 10, i.e., not on the inductance L_0, and would thus remain unchanged if this inductance were short-circuited. This means that $\hat{H}_{DI0}$ describes purely electrostatic, or capacitive, coupling. The part $\hat{H}_{DI1}$, just as $\hat{H}_{DI0}$, describes direct nonlocal coupling between the dot charges. However, in contrast to $\hat{H}_{DI0}$ the coupling strengths in $\hat{H}_{DI1}$, $\lambda_{v1}\lambda_{\mu 2}/\hbar\omega$, depend parametrically on the inductance L_0. This part is therefore electrodynamic.

As the next step we motivate the approximations leading from Eqs. (A1) and (A4) to Eq. (1), under the conditions described in the main text. To do this we use the relations $\lambda_{vi} \propto \sqrt{Z_0/R_Q}\hbar\omega$ ($Z_0 = \sqrt{L_0/C_0}$), $\omega \sim 1/\sqrt{L_0C_0}$, and $U_{v1\mu 2} \propto e^2/C_0$ for the parameters in $\hat{H}_C$. First, noting that $Z_0 \ll R_Q$ and hence $\lambda_{vi}/\hbar\omega \ll 1$ justifies a rotating-wave approximation, which amounts to neglecting all terms of $\mathcal{O}(\lambda_{vi}/\omega)$ in $\hat{H}_S$, e.g., the counter-rotating terms. Second, for the DQDs resonant with the cavity mode the direct capacitive interaction will scale as $U_{v1\mu 2}/\lambda_{v(\mu)i} \sim \sqrt{Z_0/R_Q}$ and can thus be neglected. Moreover, had we considered a full description for the transmission line DQD circuit, including all of the cavity modes, the higher frequency modes would be off-resonant with a detuning $\Delta E \gtrsim \hbar\omega$. The corrections due to this off-resonant interaction would then scale as $\lambda_{vi}/\hbar\omega$ and therefore be negligible. It should be noted that for the resonance condition to hold the tunneling amplitudes and detunings between the left and right dot orbitals the DQDs must be chosen such that $|\Delta_i| = 2\sqrt{(\hbar\omega)^2 - t^2_{LRi}}$. We further point out that the DQDi-cavity coupling strengths are $g_i = \sin(2\theta_i)(\lambda_{Ri} - \lambda_{Li})/2$. Thus, for the case of identical coupling strengths $g_1 = g_2 = g_0$, considered in the main text, the mixing angles θ_1 and θ_2 cannot be tuned independently for fixed λ_{Li} and λ_{Ri}.

APPENDIX B

We here give the explicit form for the eigenstates with a finite number of excitations in the TC subspace and all eigenenergies of $\hat{H}_S$. The former are given by

$$|D^0 1\rangle = |\mathcal{S}0\rangle\,, \quad |D^\pm 1\rangle = \frac{|gg1\rangle \pm |\mathcal{T}0\rangle}{\sqrt{2}} \tag{B1}$$

and, for $n \geqslant 2$,

$$\begin{aligned}
|D^{+-}n\rangle &= \frac{\sqrt{n-1}\,|ggn\rangle - \sqrt{n}\,|een-2\rangle}{\sqrt{2n-1}}, \\
|D^{\pm\pm}n\rangle &= \frac{\sqrt{n}\,|ggn\rangle + \sqrt{n-1}\,|een-2\rangle}{\sqrt{2(2n-1)}} \pm \frac{|\mathcal{T}n-1\rangle}{\sqrt{2}}, \\
|D^{-+}n\rangle &= |\mathcal{S}n-1\rangle\,,
\end{aligned} \tag{B2}$$

with $|\mathcal{S}(\mathcal{T})n\rangle = (|egn\rangle - (+)\,|gen\rangle)/\sqrt{2}$. The eigenenergies are

$$\epsilon_{00n} = \hbar\omega(n+1) \tag{B3}$$

for the HO subspace,

$$\epsilon_{S_i^0 0} = \hbar\omega/2, \quad \epsilon_{S_i^\pm n} = \hbar\omega(n+1/2) \pm \sqrt{n}\hbar g_0, \quad n \geqslant 1 \tag{B4}$$

for the JC subspaces, and

$$\begin{aligned}
&\epsilon_{D^0 0} = 0, \quad \epsilon_{D^0 1} = \hbar\omega, \quad \epsilon_{D^\pm 1} = \hbar\omega \pm \sqrt{2}\hbar g_0, \\
&\epsilon_{D^{\pm\pm}n} = n\hbar\omega \pm \sqrt{2(2n-1)}\hbar g_0, \quad \epsilon_{D^{\pm\mp}n} = n\hbar\omega, \quad n \geqslant 2
\end{aligned} \tag{B5}$$

for the TC subspace.

APPENDIX C

In this Appendix we explain how the QME in Eq. (3) can be reduced to a ME in the limit $\hbar g_0 \ll k_B T$, give the explicit form of the ME, and solve it in three limiting cases. We start by pointing out that in the secular regime $\Gamma_i \ll g_0$, considered here, only coherences between degenerate states, i.e., $|{+}{-}n\rangle$ and $|{-}{+}n\rangle$ need to be taken into account in the QME. Moreover, only the diagonal elements $\langle S_i^\alpha n|\hat{\rho}|S_i^\alpha n\rangle$ couple to the coherences. As pointed out in the text, for $\hbar g_0 \ll k_B T$, the QME becomes independent of g_0. This introduces additional symmetries in the QME, with two important consequences: (1) The coherences $\langle +-n|\hat{\rho}|{-}{+}n\rangle$ and $\langle -+n|\hat{\rho}|{+}{-}n\rangle$ couple with opposite signs to $\langle S_i^+ n|\hat{\rho}|S_i^+ n\rangle$ and $\langle S_i^- n|\hat{\rho}|S_i^- n\rangle$. (2) For several pairs of diagonal elements of $\hat{\rho}$, only the sums of the elements couple to the other diagonal elements. In particular, this holds for the sum $\langle S_i^+ n|\hat{\rho}|S_i^+ n\rangle + \langle S_i^- n|\hat{\rho}|S_i^- n\rangle$, to which the coherences, according to (1), do not contribute. As a result of (1) and (2), the coherences decouple from the diagonal elements of the QME, allowing us to reduce it to a standard ME.

To write the explicit form of the ME it is convenient to first introduce a shorthand notation for the diagonal elements of $\hat{\rho}$, i.e., the probabilities for the eigenstates of $\hat{H}_S$. The probabilities, or the sums of probabilities, for states the HO, JC, and TC subspaces are denoted by

$$\begin{aligned}
P^n_{00} &= \langle 00n|\hat{\rho}|00n\rangle\,, \\
P^n_{S_i} &= \delta_{n0}\langle S_i^0 0|\hat{\rho}|S_i^0 0\rangle + (1-\delta_{n0})\sum_{\alpha=\pm}\langle S_i^\alpha n|\hat{\rho}|S_i^\alpha n\rangle
\end{aligned} \tag{C1}$$

and

$$\begin{aligned}
P^n_D &= \delta_{n0}\,\langle D^0 0|\hat{\rho}|D^0 0\rangle + \delta_{n1}\sum_{\alpha=\pm}\langle D^\alpha 1|\hat{\rho}|D^\alpha 1\rangle \\
&\quad + (1-\delta_{n0}-\delta_{n1})\sum_{\alpha=\pm}\langle D^{\alpha\alpha}n|\hat{\rho}|D^{\alpha\alpha}n\rangle\,, \\
P^1_{D^0} &= \langle D^0 1|\hat{\rho}|D^0 1\rangle\,, \\
P^n_{D^{+-(-+)}} &= \langle D^{+-(-+)}n|\hat{\rho}|D^{+-(-+)}n\rangle\,, \quad n \geqslant 2,
\end{aligned} \tag{C2}$$

respectively. By further introducing vectors $\mathbf{P}_X = (P^0_X \;\; P^1_X \;\; P^2_X \;\; \cdots)^T$, with $X = 00, S_1, S_2$, containing the probabilities for states with one or both DQDs unoccupied and vectors $\mathbf{P}_D = (P^2_D \;\; P^3_D \;\; \cdots)^T$ and $\mathbf{P}_{D^{+-(-+)}} = (P^2_{D^{+-(-+)}} \;\; P^3_{D^{+-(-+)}} \;\; \cdots)^T$ containing the probabilities for states with both DQDs occupied, the

ME can be written

$$\frac{d}{dt}\underbrace{\begin{pmatrix}\mathbf{P}_{00}\\ \mathbf{P}_{S_1}\\ \mathbf{P}_{S_2}\\ P^0_D\\ P^1_{D^0}\\ P^1_D\\ \mathbf{P}_D\\ \mathbf{P}_{D^{+-}}\\ \mathbf{P}_{D^{-+}}\end{pmatrix}}_{P} = \underbrace{\begin{pmatrix} M_{00} & M^{00}_{S_1} & M^{00}_{S_2} & 0 & 0 & 0 & 0 & 0 & 0\\ M^{S_1}_{00} & M_{S_1} & 0 & M^{S_1}_{D0} & M^{S_1}_{D^01} & M^{S_1}_{D1} & M^{S_1}_{D} & M^{S_1}_{D^{+-}} & M^{S_1}_{D^{-+}}\\ M^{S_2}_{00} & 0 & M_{S_2} & M^{S_2}_{D0} & M^{S_2}_{D^01} & M^{S_2}_{D1} & M^{S_2}_{D} & M^{S_2}_{D^{+-}} & M^{S_2}_{D^{-+}}\\ 0 & M^{D0}_{S_1} & M^{D0}_{S_2} & M_{D0} & 0 & 0 & 0 & 0 & 0\\ 0 & M^{D^01}_{S_1} & M^{D^01}_{S_2} & 0 & M_{D^01} & 0 & 0 & 0 & 0\\ 0 & M^{D1}_{S_1} & M^{D1}_{S_2} & 0 & 0 & M_{D1} & 0 & 0 & 0\\ 0 & M^{D}_{S_1} & M^{D}_{S_2} & 0 & 0 & 0 & M_D & 0 & 0\\ 0 & M^{D^{+-}}_{S_1} & M^{D^{+-}}_{S_2} & 0 & 0 & 0 & 0 & M_{D^{+-}} & 0\\ 0 & M^{D^{-+}}_{S_1} & M^{D^{-+}}_{S_2} & 0 & 0 & 0 & 0 & 0 & M_{D^{-+}}\end{pmatrix}}_{M}\begin{pmatrix}\mathbf{P}_{00}\\ \mathbf{P}_{S_1}\\ \mathbf{P}_{S_2}\\ P^0_D\\ P^1_{D^0}\\ P^1_D\\ \mathbf{P}_D\\ \mathbf{P}_{D^{+-}}\\ \mathbf{P}_{D^{-+}}\end{pmatrix}. \tag{C3}$$

The submatrices in M below and above the diagonal are here given by

$$\begin{aligned}&\left(M^{S_i}_{00}\right)_{nm} = \sum_{j=0,1}\delta_{nm+j}\mathcal{G}^j_i, \quad \left(M^{Y}_{S_i}\right)_{nm} = \sum_{j=0,1}\delta_{n+1+jm}x^Y_{nj}\mathcal{G}^{1-j}_{\bar{i}}, \quad x^D_{nj} = \frac{4n+1+2j}{4(2n+1)}, \quad x^{D^{+-}}_{nj} = \frac{n+1-j}{2(2n+1)}, \quad x^{D^{-+}}_{nj} = \frac{1}{4}\\ &\left(M^{D0}_{S_i}\right)_{1m} = \delta_{1m}\mathcal{G}^0_{\bar{i}}, \quad \left(M^{D^01}_{S_i}\right)_{1m} = \delta_{1m}\mathcal{G}^1_{\bar{i}}/2 + \delta_{2m}\mathcal{G}^0_{\bar{i}}/4, \quad \left(M^{D1}_{S_i}\right)_{1m} = \delta_{1m}\mathcal{G}^1_{\bar{i}}/2 + 3\delta_{2m}\mathcal{G}^0_{\bar{i}}/4,\end{aligned} \tag{C4}$$

and

$$\begin{aligned}&\left(M^{00}_{S_i}\right)_{nm} = \sum_{j=0,1}\frac{\delta_{n+jm}}{2-\delta_{n1}\delta_{j0}}\tilde{\mathcal{G}}^j_i, \quad \left(M^{S_i}_{Z}\right)_{nm} = \sum_{j=0,1}\delta_{nm+1+j}y^Z_{nj}\tilde{\mathcal{G}}^{1-j}_{\bar{i}},\\ &y^D_{nj} = \frac{(4n-3-2j)}{4(2n-1-2j)}, \quad y^{D^{+-}}_{nj} = \frac{n-2j}{2n-1-2j}, \quad y^{D^{-+}}_{nj} = \frac{1}{2},\\ &\left(M^{S_i}_{D0}\right)_{n1} = \delta_{n1}\tilde{\mathcal{G}}^0_{\bar{i}}, \quad \left(M^{S_i}_{D^01}\right)_{n1} = \delta_{n1}\tilde{\mathcal{G}}^1_{\bar{i}}/2 + \delta_{n2}\tilde{\mathcal{G}}^0_{\bar{i}}/2, \quad \left(M^{S_i}_{D1}\right)_{n1} = \delta_{n1}\tilde{\mathcal{G}}^1_{\bar{i}}/4 + \delta_{n2}3\tilde{\mathcal{G}}^0_{\bar{i}}/4,\end{aligned} \tag{C5}$$

respectively. Here $\mathcal{G}^0_i = \sum_\nu \bar{\Gamma}_{\nu gi} f_{\nu i}(-\hbar\omega/2)$, $\mathcal{G}^1_i = \sum_\nu \bar{\Gamma}_{\nu ei} f_{\nu i}(\hbar\omega/2)$, $\tilde{\mathcal{G}}^0_i = \sum_\nu \bar{\Gamma}_{\nu gi} \tilde{f}_{\nu i}(-\hbar\omega/2)$, and $\tilde{\mathcal{G}}^1_i = \sum_\nu \bar{\Gamma}_{\nu ei} \tilde{f}_{\nu i}(\hbar\omega/2)$, and we use the i-index convention $\bar{1}=2$ and $\bar{2}=1$. The submatrices on the diagonal in M are diagonal with elements such that the sum of every column in M is zero. This structure ensures that the ME conserves probability.

We find the steady-state solution to the ME in Eq. (C3) analytically in three limiting cases:

(i) For $\theta_1=\theta_2$, symmetric bias voltages $eV_1, eV_2 \gg \hbar\omega$ applied across both DQD1 and DQD2.

(ii) For the bias condition of Sec. III with $\Gamma_1 \gg \Gamma_2$ and symmetric bias voltage across DQD1. Here we calculate the distribution to zeroth order in Γ_2/Γ_1.

(iii) For the bias condition of Sec. III with $\Gamma_2 \gg \Gamma_1$ and symmetric bias voltage across DQD1. The distribution is here calculated to first order in Γ_1/Γ_2.

The solution for case (i) is used to derive the stability condition in Sec. II B, while the solutions for the cases (ii) and (iii) are used to obtain the analytical expression for the current in DQD2, correct to first order in Γ_2/Γ_1 and Γ_1/Γ_2, respectively (see Sec. III).

To find the solution of the ME in case (i) we use a general property of the ME. This property states that $P^n_{S_1}$ and $P^n_{S_2}$ will couple only to the probabilities for states with both DQDs unoccupied having n or $n+1$ excitations and for states with both DQDs occupied having n or $n-1$ excitations (see Fig. 2). In turn the probabilities for these states will couple to $P^{n+k}_{S_1}$ and $P^{n+k}_{S_2}$, with $k=-1,0,1$. Two coupled second-order difference equations are thus obtained for the probabilities in $\mathbf{P}_{S_1}$ and $\mathbf{P}_{S_2}$. For the special conditions (i) these difference equations become particularly simply. Introducing the vector $\tilde{\mathbf{P}}_n = (P^n_{S_1}\ P^n_{S_2})^T$, these equation be written

$$\begin{aligned}\sin^4(\theta)M_0\tilde{\mathbf{P}}_1 &= (2\cos^4(\theta)M_0 + [1+\cos^2(\theta)]B)\tilde{\mathbf{P}}_0,\\ \sin^4(\theta)M_1\tilde{\mathbf{P}}_2 &= \left[\cos^4(\theta)M_1 + \cos^4(\theta)M_0 + \frac{3B}{2}\right]\tilde{\mathbf{P}}_1\\ &\quad - 2\cos^4(\theta)M_0\tilde{\mathbf{P}}_0,\\ \sin^4(\theta)M_n\tilde{\mathbf{P}}_{n+1} &= \left[\cos^4(\theta)M_n + \sin^4(\theta)M_{n-1} + \frac{3B}{2}\right]\tilde{\mathbf{P}}_n\\ &\quad - \cos^4(\theta)M_{n-1}\tilde{\mathbf{P}}_{n-1}, \quad n \geqslant 2,\end{aligned} \tag{C6}$$

with

$$\begin{aligned}B &= \Gamma_1\Gamma_2\begin{pmatrix}1 & -1\\ -1 & 1\end{pmatrix},\\ M_n &= \begin{pmatrix}\Gamma_1^2/2 + \Gamma_2^2 b_n & \Gamma_1\Gamma_2(1/2+b_n)\\ \Gamma_1\Gamma_2(1/2+b_n) & \Gamma_2^2/2 + \Gamma_1^2 b_n\end{pmatrix},\end{aligned} \tag{C7}$$

and

$$\begin{aligned}b_n &= \frac{(4n+3)(4n+1)}{4(2n+1)[4n+1+2\cos^2(\theta)]} + \frac{1}{4}\\ &\quad + \frac{n(n+1)}{2(2n+1)[n+\sin^2(\theta)]}.\end{aligned} \tag{C8}$$

Together with the condition $\tilde{\mathbf{P}}_n \to 0$ for $n \to \infty$, Eq. (C6) has the solution $\tilde{\mathbf{P}}_n = \cot^{4n+2}(\theta)(1 \quad 1)^T P^0_{11}$, independent of Γ_1 and Γ_2. This solution is then used to find the probabilities for the states with both DQDs occupied and unoccupied, respectively. Requiring that the solution to Eq. (C3) be normalized we get

$$\begin{aligned} &P^n_{00} = \cot^{4(n+1)}(\theta)x_0, \quad P^0_{S_i} = \cot^2(\theta)x_0, \\ &P^n_{S_i} = 2\cot^{4n+2}(\theta)x_0, \quad n \geqslant 1, \\ &P^0_D = x_0, \quad P^1_D = 2P^1_{D^0} = 2\cot^4(\theta)x_0, \\ &P^n_D = 2P^n_{D^{+-(-+)}} = 2\cot^{4n}(\theta)x_0, \quad n \geqslant 2, \end{aligned} \tag{C9}$$

with $x_0 = [1 - \cot^4(\theta)]/[1 + \cot^2(\theta) + \cot^4(\theta)]^2$. It is clear from Eq. (C9) that a well defined solution, or equivalently a solution with noninfinite mean number of excitations, exists if $\theta > \pi/4$. On physical grounds we argue that there exists a more general stability condition applying also for mixing angles $\theta_1 \neq \theta_2$. We start by considering the case when $\theta_1 = \theta_2 > \pi/4$ and one of the mixing angles is increased. From the discussion below Eq. (3) it is clear that this will increase absorption relative to emission of photons by tunneling electrons. The mean number of excitations will then be decreased and the distribution must therefore still be convergent. Since all pairs of mixing angles $\theta_1, \theta_2 > \pi/4$ can be reached this way it follows that a well defined solution exists for all of them. The mean number of excitations will also decrease if the bias voltage is decreased. The stability condition, $\theta_1, \theta_2 > \pi/4$, must therefore also hold for finite bias voltages. This conclusion is further supported by numerical investigations.

In the limiting case (ii) the relation between probabilities for states with DQD2 unoccupied, e.g., P^n_{00} and P^m_{S1}, are entirely determined by the tunneling in DQD1. Similarly the tunneling in DQD1 entirely determines the relation between probabilities for states with DQD2 occupied. The tunneling in DQD2 only effects the total probability for DQD2 being occupied. The main steps in the solution of the ME in this limit are most clearly visualized by rewriting $M\mathbf{P} = 0$ as

$$\underbrace{\begin{pmatrix} \bar{M}^{(0)}_{00} + \Gamma_2/\Gamma_1 \bar{M}^{(1)}_{00} & \Gamma_2/\Gamma_1 \bar{M}^{(1)}_{10} \\ \Gamma_2/\Gamma_1 \bar{M}^{(1)}_{01} & \bar{M}^{(0)}_{11} + \Gamma_2/\Gamma_1 \bar{M}^{(1)}_{11} \end{pmatrix}}_{\bar{M}} \underbrace{\begin{pmatrix} \bar{\mathbf{P}}_{20} \\ \bar{\mathbf{P}}_{21} \end{pmatrix}}_{\bar{\mathbf{P}}} = 0, \tag{C10}$$

where the vectors $\bar{\mathbf{P}}_{20}$ and $\bar{\mathbf{P}}_{21}$ contain the probabilities for states with DQD2 unoccupied and occupied, respectively. The matrix $\bar{M}$ further contains the transition rates in M divided by Γ_1. The starting point of the derivation is to note that for $\Gamma_2 = 0$ the matrix is block-diagonal, with blocks $\bar{M}^{(0)}_{ii}$, and that $\det(\bar{M}^{(0)}_{ii}) = 0$. It then follows that the eigenvalue zero of the matrix $\bar{M}$ is doubly degenerate for $\Gamma_2 = 0$. To find the solution $\bar{\mathbf{P}}^{(0)}$ to Eq. (C10) to zeroth order in Γ_2/Γ_1, i.e., the limit of $\bar{\mathbf{P}}$ as $\Gamma_2/\Gamma_1 \to 0$, we must therefore apply degenerate perturbation theory generalized to ME matrices. The first step in this procedure is to find the two linearly independent solutions to Eq. (C10), i.e., the eigenvectors corresponding to the eigenvalue zero of $\bar{M}$. Setting $\Gamma_2 = 0$ in the equation, the two linearly independent eigenvectors acquire the forms $\bar{\mathbf{P}}_0 = (\bar{\mathbf{P}}^{(0)}_{20} \; 0)^T$ and $\bar{\mathbf{P}}_1 = (0 \; \bar{\mathbf{P}}^{(0)}_{21})^T$, where $\bar{\mathbf{P}}^{(0)}_{20}$ and $\bar{\mathbf{P}}^{(0)}_{21}$ fulfill the equations $M^{(0)}_{00}\bar{\mathbf{P}}^{(0)}_{20} = 0$ and $M^{(0)}_{11}\bar{\mathbf{P}}^{(0)}_{21} = 0$, respectively. Importantly these equations can readily be solved analytically as they give difference equations similar to Eq. (C6). The next step is to express $\bar{\mathbf{P}}^{(0)}$ as a normalized linear combination of these vectors, i.e., $c_0\bar{\mathbf{P}}_0 + c_1\bar{\mathbf{P}}_1$, to which $\bar{\mathbf{P}}$ tend as $\Gamma_2/\Gamma_1 \to 0$. To this aim we define the projectors $\mathcal{P} = \bar{\mathbf{P}}_0(U_0 \; 0) + \bar{\mathbf{P}}_1(0 \; U_1)$ and $\mathcal{Q} = 1 - \mathcal{P}$. Here $(U_0 \; 0)$ and $(0 \; U_1)$, with $U_i = (1 \; 1 \; \ldots)$, are the left eigenvectors to the eigenvalue zero in $\bar{M}$ normalized so that $U_i\bar{\mathbf{P}}_{2i} = 1$. Then by applying the steps presented in Ref. 80 the equation $\mathcal{P}M^{(1)}\mathcal{P}\bar{\mathbf{P}}^{(0)} = 0$ for $\bar{\mathbf{P}}^{(0)}$ is obtained. In turn this equation gives

$$c_0U_0\bar{M}_{00}\bar{\mathbf{P}}^{(0)}_{20} + c_1U_0\bar{M}_{10}\bar{\mathbf{P}}^{(0)}_{21} = 0, \tag{C11}$$

which together with the normalization condition $c_0 + c_1 = 1$, determines c_0 and c_1. The different elements in $\bar{\mathbf{P}}^{(0)}$ can then be written

$$\begin{aligned} &P^n_{00} = [\gamma/(1-\gamma)]^{2n+1}\tilde{c}_0, \\ &P^n_{S_1} = (2 - \delta_{n0})[\gamma/(1-\gamma)]^{2n}\tilde{c}_0, \\ &P^n_{S_2} = (2 - \delta_{n0})[\gamma/(1-\gamma)]^{2n+1}\tilde{c}_1, \\ &P^0_D = \tilde{c}_1, \quad P^1_D = 2P^{01}_{D^0} = 2[\gamma/(1-\gamma)]^2\tilde{c}_1, \\ &P^n_D = 2P^n_{D^{+-(-+)}} = 2[\gamma/(1-\gamma)]^{2n}\tilde{c}_1, \quad n \geqslant 2, \end{aligned} \tag{C12}$$

where

$$\begin{aligned} \tilde{c}_0 &= \frac{\eta\gamma^2}{(1 - 2\gamma + 2\gamma^2)[1 + 2\cot^2(\theta_2)] + \gamma^2}, \\ \tilde{c}_1 &= \frac{\eta(1-\gamma)^2[1 + 2\cot^2(\theta_2)]}{(1 - 2\gamma + 2\gamma^2)[1 + 2\cot^2(\theta_2)] + \gamma^2}, \end{aligned} \tag{C13}$$

and $\eta = (1 - 2\gamma)/(1 - \gamma + \gamma^2)$. With the probabilities in Eq. (C12) and the rates between DQD2 and its right lead for the corresponding states it is straightforward to derive the second expression for the current through DQD2 in Eq. (4).

To solve the ME in case (iii) we first recall, from the main text, that only the state and transitions depicted in Fig. 6 contribute to the transport quantities to first order in Γ_1/Γ_2. We then focus on the corresponding effective ME $M_e\mathbf{P}_e = 0$ for the probabilities $\mathbf{P}_e$ for these states, taking only the additional transitions $\{|D^{\alpha 1}\rangle\} \to |S^0_2\rangle$ into account. To first order in Γ_1/Γ_2 we get

$$\begin{aligned} P^0_D &= \frac{1}{1+\gamma} - \frac{\Gamma_1}{\Gamma_2}\frac{2[2 + \cos^2(\theta_2)]}{\sin^2(\theta_2)}\frac{\gamma^2}{(1+\gamma)^2} \\ &\quad - \frac{\Gamma_1}{\Gamma_2}\frac{[1 + \cos^2(\theta_2)]}{\sin^2(\theta_2)}\frac{\gamma^2(1-\gamma)}{(1+\gamma)^2}, \\ P^0_{S_2} &= \frac{\gamma}{1+\gamma} - \frac{\Gamma_1}{\Gamma_2}\frac{2[2 + \cos^2(\theta_2)]}{\sin^2(\theta_2)}\frac{\gamma^3}{(1+\gamma)^2} \\ &\quad + \frac{\Gamma_1}{\Gamma_2}\frac{[1 + \cos^2(\theta_2)]}{\sin^2(\theta_2)}\frac{\gamma^2(1-\gamma)}{(1+\gamma)^2}, \\ P^1_D &= 2P^1_{D^0} = \frac{2\Gamma_1}{\Gamma_2}\frac{1 + \cos^2(\theta_2)}{\sin^2(\theta_2)}\frac{\gamma^2}{(1+\gamma)}, \\ P^0_{S_1} &= \frac{\Gamma_1}{\Gamma_2}\frac{\gamma^2}{(1+\gamma)}. \end{aligned} \tag{C14}$$

These probabilities are used to obtain the first expression for current through DQD2 in Eq. (4).

APPENDIX D

In this Appendix we present the derivation of currents, current correlations, as well as the full statistics of charge transfer across the DQDs. Following the procedure of Refs. 81 and 82 we rewrite the QME of Eq. (3) in the n-resolved form and Fourier transform it with respect to the number of electrons having tunneled through DQD1 and DQD2. The QME then transforms to $d\hat{\rho}/dt = \mathcal{L}(\chi_1,\chi_2)\hat{\rho}$, where the counting fields χ_1 and χ_2 are the conjugate variables to the number of electrons having tunneled through DQD1 and DQD2. The eigenvalue of $\mathcal{L}(\chi_1,\chi_2)$ tending to zero as $\chi_1,\chi_2 \to 0$ is the long time limit cumulant generating function $\mathcal{F}(\chi_1,\chi_2)$. The currents and the noise are obtained from the first and second derivatives of $\mathcal{F}(\chi_1,\chi_2)$, i.e., $I_i = e\partial_{i\chi_i}\mathcal{F}|_{\chi_1=\chi_2=0}$ and $S_{ij} = e^2\partial_{i\chi_i}\partial_{i\chi_j}\mathcal{F}|_{\chi_1=\chi_2=0}$. These quantities can conveniently be accessed via the eigenvalue problem $\mathcal{L}(\chi_1,\chi_2)[\hat{\rho}(\chi_1,\chi_2)] = \mathcal{F}(\chi_1,\chi_2)\hat{\rho}(\chi_1,\chi_2)$. In the present paper this full QME approach is used only to calculate the current in Fig. 7.

In the ME limit the eigenvalue problem above reads $M(\chi_1,\chi_2)\mathbf{P}(\chi_1,\chi_2) = \mathcal{F}(\chi_1,\chi_2)\mathbf{P}(\chi_1,\chi_2)$. We use this equation to calculate the noise plotted in Fig. 5. We also use the equation to obtain the CGF of Eq. (6), i.e., the CGF to first order in Γ_1/Γ_2 for the bias condition of DQD2 described in Sec. III with DQD1 in the high-bias regime. To do this we write $\det[M(\chi_1,\chi_2) - \mathcal{F}(\chi_1,\chi_2)] = 0$ as

$$\det\begin{pmatrix} M_e(\chi_1,\chi_2) - \mathcal{F} & M_{r\to e}(\chi_1,\chi_2) \\ M_{e\to r}(\chi_1,\chi_2) & M_r(\chi_1,\chi_2) - \mathcal{F} \end{pmatrix} = 0. \quad \text{(D1)}$$

Here $M_{e\to r}$, $M_{r\to e}$, and M_r are matrices describing the transitions to, from, and within the subspace of states not included in the Fig. 6. Importantly, $(M_{e\to r})_{nm} \propto \mathcal{O}(\Gamma_1/\Gamma_2)$ and $(M_{r\to e})_{nm} \propto \mathcal{O}(1)$. This means that

$$\det[M_e(\chi_1,\chi_2) - \mathcal{F}^{(1)}(\chi_1,\chi_2)] = 0, \quad \text{(D2)}$$

where $\mathcal{F}^{(1)}(\chi_1,\chi_2)$ is the CGF to first order in Γ_1/Γ_2. Dropping terms of $\mathcal{O}[(\Gamma_1/\Gamma_2)^2]$ in Eq. (D2) and solving for $\mathcal{F}^{(1)}$ then gives Eq. (6).

[1] A. Blais, R. S. Huang, A. Wallraff, S. M. Girvin, and R. J. Schoelkopf, Phys. Rev. A **69**, 062320 (2004).
[2] A. Wallraff, D. Schuster, A. Blais, L. Frunzio, R. Huang, J. Majer, S. Kumar, S. Girvin, and R. Schoelkopf, Nature (London) **431**, 162 (2004).
[3] R. Schoelkopf and S. Girvin, Nature (London) **451**, 664 (2008).
[4] M. Sillanpää, J. Park, and R. Simmonds, Nature (London) **449**, 438 (2007).
[5] J. Majer, J. Chow, J. Gambetta, J. Koch, B. Johnson, J. Schreier, L. Frunzio, D. Schuster, A. Houck, A. Wallraff *et al.*, Nature (London) **449**, 443 (2007).
[6] L. DiCarlo, J. Chow, J. Gambetta, L. Bishop, B. Johnson, D. Schuster, J. Majer, A. Blais, L. Frunzio, S. Girvin *et al.*, Nature (London) **460**, 240 (2009).
[7] L. DiCarlo, M. Reed, L. Sun, B. Johnson, J. Chow, J. Gambetta, L. Frunzio, S. Girvin, M. Devoret, and R. Schoelkopf, Nature (London) **467**, 574 (2010).
[8] A. Houck, D. Schuster, J. Gambetta, J. Schreier, B. Johnson, J. Chow, J. Majer, L. Frunzio, M. Devoret, S. Girvin *et al.*, Nature (London) **449**, 328 (2007).
[9] M. Hofheinz, E. Weig, M. Ansmann, R. Bialczak, E. Lucero, M. Neeley, A. O'Connell, H. Wang, J. Martinis, and A. Cleland, Nature (London) **454**, 310 (2008).
[10] M. Hofheinz, H. Wang, M. Ansmann, R. Bialczak, E. Lucero, M. Neeley, A. O'Connell, D. Sank, J. Wenner, J. Martinis *et al.*, Nature (London) **459**, 546 (2009).
[11] C. Eichler, D. Bozyigit, C. Lang, L. Steffen, J. Fink, and A. Wallraff, Phys. Rev. Lett. **106**, 220503 (2011).
[12] C. Eichler, D. Bozyigit, C. Lang, M. Baur, L. Steffen, J. M. Fink, S. Filipp, and A. Wallraff, Phys. Rev. Lett. **107**, 113601 (2011).
[13] H. Wang, M. Mariantoni, R. C. Bialczak, M. Lenander, E. Lucero, M. Neeley, A. D. O'Connell, D. Sank, M. Weides, J. Wenner *et al.*, Phys. Rev. Lett. **106**, 060401 (2011).
[14] Z.-L. Xiang, S. Ashhab, J. Q. You, and F. Nori, Rev. Mod. Phys. **85**, 623 (2013).
[15] J. Koch, A. A. Houck, K. L. Hur, and S. M. Girvin, Phys. Rev. A **82**, 043811 (2010).
[16] J. R. Johansson, G. Johansson, C. M. Wilson, and F. Nori, Phys. Rev. Lett. **103**, 147003 (2009).
[17] C. Wilson, G. Johansson, A. Pourkabirian, M. Simoen, J. Johansson, T. Duty, F. Nori, and P. Delsing, Nature (London) **479**, 376 (2011).
[18] R. Vijay, D. H. Slichter, and I. Siddiqi, Phys. Rev. Lett. **106**, 110502 (2011).
[19] L. Childress, A. S. Sørensen, and M. D. Lukin, Phys. Rev. A **69**, 042302 (2004).
[20] G. Burkard and A. Imamoglu, Phys. Rev. B **74**, 041307(R) (2006).
[21] O. Astafiev, K. Inomata, A. Niskanen, N. Y. Pashkin, Yu. A, and J. Tsai, Nature (London) **449**, 588 (2007).
[22] M. Trif, V. N. Golovach, and D. Loss, Phys. Rev. B **77**, 045434 (2008).
[23] G.-P. Guo, H. Zhang, Y. Hu, T. Tu, and G.-C. Guo, Phys. Rev. A **78**, 020302(R) (2008).
[24] M. Marthaler, G. Schön, and A. Shnirman, Phys. Rev. Lett. **101**, 147001 (2008).
[25] N. Lambert and F. Nori, Phys. Rev. B **78**, 214302 (2008).
[26] N. Lambert, Y.-n. Chen, R. Johansson, and F. Nori, Phys. Rev. B **80**, 165308 (2009).
[27] A. Cottet, C. Mora, and T. Kontos, Phys. Rev. B **83**, 121311 (2011).
[28] J. Basset, H. Bouchiat, and R. Deblock, Phys. Rev. Lett. **105**, 166801 (2010).
[29] M. Hofheinz, F. Portier, Q. Baudouin, P. Joyez, D. Vion, P. Bertet, P. Roche, and D. Esteve, Phys. Rev. Lett. **106**, 217005 (2011).
[30] T. Frey, P. Leek, M. Beck, K. Ensslin, A. Wallraff, and T. Ihn, Appl. Phys. Lett. **98**, 262105 (2011).
[31] M. R. Delbecq, V. Schmitt, F. D. Parmentier, N. Roch, J. J. Viennot, G. Fève, B. Huard, C. Mora, A. Cottet, and T. Kontos, Phys. Rev. Lett. **107**, 256804 (2011).

[32]A. Cottet and T. Kontos, Phys. Rev. Lett. **105**, 160502 (2010).
[33]P.-Q. Jin, M. Marthaler, J. H. Cole, A. Shnirman, and G. Schön, Phys. Rev. B **84**, 035322 (2011).
[34]C. Bergenfeldt and P. Samuelsson, Phys. Rev. B **85**, 045446 (2012).
[35]A. Cottet, T. Kontos, and A. L. Yeyati, Phys. Rev. Lett. **108**, 166803 (2012).
[36]P.-Q. Jin, M. Marthaler, A. Shnirman, and G. Schön, Phys. Rev. Lett. **108**, 190506 (2012).
[37]T. Frey, P. J. Leek, M. Beck, J. Faist, A. Wallraff, K. Ensslin, T. Ihn, and M. Büttiker, Phys. Rev. B **86**, 115303 (2012).
[38]I. Chernii and E. V. Sukhorukov, Phys. Rev. B **85**, 205438 (2012).
[39]T. Frey, P. J. Leek, M. Beck, A. Blais, T. Ihn, K. Ensslin, and A. Wallraff, Phys. Rev. Lett. **108**, 046807 (2012).
[40]H. Toida, T. Nakajima, and S. Komiyama, Phys. Rev. Lett. **110**, 066802 (2013).
[41]K. Petersson, L. McFaul, M. Schroer, M. Jung, J. Taylor, A. Houck, and J. Petta, Nature (London) **490**, 380 (2012).
[42]M. Delbecq, L. Bruhat, J. Viennot, S. Datta, A. Cottet, and T. Kontos, Nat. Commun. **4**, 1400 (2013).
[43]A. Wallraff, A. Stockklauser, T. Ihn, J. R. Petta, and A. Blais, arXiv:1304.3697.
[44]M. Sandberg, C. Wilson, F. Persson, T. Bauch, G. Johansson, V. Shumeiko, T. Duty, and P. Delsing, Appl. Phys. Lett. **92**, 203501 (2008).
[45]C. M. Wilson, T. Duty, M. Sandberg, F. Persson, V. Shumeiko, and P. Delsing, Phys. Rev. Lett. **105**, 233907 (2010).
[46]N. M. Chtchelkatchev, G. Blatter, G. B. Lesovik, and T. Martin, Phys. Rev. B **66**, 161320 (2002).
[47]P. Samuelsson, E. V. Sukhorukov, and M. Büttiker, Phys. Rev. Lett. **91**, 157002 (2003).
[48]C. W. J. Beenakker, C. Emary, M. Kindermann, and J. L. van Velsen, Phys. Rev. Lett. **91**, 147901 (2003).
[49]P. Samuelsson, E. V. Sukhorukov, and M. Büttiker, Phys. Rev. Lett. **92**, 026805 (2004).
[50]M. Meschke, W. Guichard, and J. Pekola, Nature (London) **444**, 187 (2006).
[51]A. V. Timofeev, M. Helle, M. Meschke, M. Möttönen, and J. P. Pekola, Phys. Rev. Lett. **102**, 200801 (2009).
[52]M. Tavis and F. W. Cummings, Phys. Rev. **170**, 379 (1968).
[53]J. M. Fink, R. Bianchetti, M. Baur, M. Göppl, L. Steffen, S. Filipp, P. J. Leek, A. Blais, and A. Wallraff, Phys. Rev. Lett. **103**, 083601 (2009).
[54]T. Vorrath and T. Brandes, Phys. Rev. B **68**, 035309 (2003).
[55]L. D. Contreras-Pulido and R. Aguado, Phys. Rev. B **77**, 155420 (2008).
[56]C. Gardiner and P. Zoller, *Quantum Noise* (Springer-Verlag, Berlin, 2004).
[57]T. Brandes and N. Lambert, Phys. Rev. B **67**, 125323 (2003).
[58]D. A. Rodrigues, J. Imbers, and A. D. Armour, Phys. Rev. Lett. **98**, 067204 (2007).
[59]S. Ashhab, J. Johansson, A. Zagoskin, and F. Nori, New J. Phys. **11**, 023030 (2009).
[60]M. Marthaler, J. Leppäkangas, and J. H. Cole, Phys. Rev. B **83**, 180505 (2011).
[61]Y. Blanter and M. Büttiker, Phys. Rep. **336**, 1 (2000).
[62]A. Cottet, W. Belzig, and C. Bruder, Phys. Rev. Lett. **92**, 206801 (2004).
[63]W. Belzig, Phys. Rev. B **71**, 161301 (2005).
[64]D. A. Bagrets and Y. V. Nazarov, Phys. Rev. B **67**, 085316 (2003).
[65]W. K. Wootters, Phys. Rev. Lett. **80**, 2245 (1998).
[66]B. Trauzettel, A. N. Jordan, C. W. J. Beenakker, and M. Büttiker, Phys. Rev. B **73**, 235331 (2006).
[67]N. Lambert, R. Aguado, and T. Brandes, Phys. Rev. B **75**, 045340 (2007).
[68]C. Emary, Phys. Rev. B **80**, 161309 (2009).
[69]C. Nietner, G. Schaller, C. Pöltl, and T. Brandes, Phys. Rev. B **85**, 245431 (2012).
[70]M. A. Nielsen and I. L. Chuang, *Quantum Computation and Quantum Information* (Cambridge University Press, Cambridge, UK, 2010).
[71]M. Castellanos-Beltran and K. Lehnert, Appl. Phys. Lett. **91**, 083509 (2007).
[72]M. Castellanos-Beltran, K. Irwin, G. Hilton, L. Vale, and K. Lehnert, Nat. Phys. **4**, 929 (2008).
[73]N. A. Masluk, I. M. Pop, A. Kamal, Z. K. Minev, and M. H. Devoret, Phys. Rev. Lett. **109**, 137002 (2012).
[74]A. Cottet and T. Kontos, Phys. Rev. Lett. **105**, 160502 (2010).
[75]W. G. van der Wiel, S. De Franceschi, J. M. Elzerman, T. Fujisawa, S. Tarucha, and L. P. Kouwenhoven, Rev. Mod. Phys. **75**, 1 (2002).
[76]M. Devoret, *Quantum Fluctuations, Les Houches Session LXIII, 1997*, edited by S. Reynaud, E. Giacobino, and J. Zinn-Justin (Elsevier, Amsterdam, 1997).
[77]E. Paladino, F. Taddei, G. Giaquinta, and G. Falci, Physica E **18**, 39 (2003).
[78]M. Devoret, S. Girvin, and R. Schoelkopf, Ann. Phys. (NY) **16**, 767 (2007).
[79]A. Mitra, I. Aleiner, and A. J. Millis, Phys. Rev. B **69**, 245302 (2004).
[80]J. Sakurai, *Modern Quantum Mechanics* (Addison-Wesley, Reading, MA, 1994).
[81]C. Flindt, T. Novotný, and A. Jauho, Europhys. Lett. **69**, 475 (2005).
[82]G. Kießlich, P. Samuelsson, A. Wacker, and E. Schöll, Phys. Rev. B **73**, 033312 (2006).
[83]N. Lambert, C. Flindt, and F. Nori, arXiv:1303.7449.
[84]L. D. Contreras-Pulido, C. Emary, T. Brandes, and R. Aguado, arXiv:1304.7192.